

Highly Sensitive Printed Accelerometer for Biomedical Applications

by

Yuanfeng Zhang

B.Eng., Zhejiang University, 2012

Thesis Submitted in Partial Fulfillment of the
Requirements for the Degree of
Master of Applied Science

in the

School of Mechatronic Systems Engineering
Faculty of Applied Science

© Yuanfeng Zhang 2014

SIMON FRASER UNIVERSITY

Summer 2014

All rights reserved.

However, in accordance with the *Copyright Act of Canada*, this work may be reproduced, without authorization, under the conditions for "Fair Dealing." Therefore, limited reproduction of this work for the purposes of private study, research, criticism, review and news reporting is likely to be in accordance with the law, particularly if cited appropriately.

Approval

Name: Yuanfeng Zhang
Degree: Master of Applied Science
Title: *Highly Sensitive Printed Accelerometer for Biomedical Applications*
Examining Committee: Chair: Dr. Siamak Arzanpour
Associate Professor

Dr. Woo Soo Kim
Senior Supervisor
Assistant Professor

Dr. Carlo Menon
Supervisor
Associate Professor

Dr. Carolyn Sparrey
Internal Examiner
Assistant Professor

Date Defended: May 27, 2014

Partial Copyright Licence



The author, whose copyright is declared on the title page of this work, has granted to Simon Fraser University the non-exclusive, royalty-free right to include a digital copy of this thesis, project or extended essay[s] and associated supplemental files (“Work”) (title[s] below) in Summit, the Institutional Research Repository at SFU. SFU may also make copies of the Work for purposes of a scholarly or research nature; for users of the SFU Library; or in response to a request from another library, or educational institution, on SFU’s own behalf or for one of its users. Distribution may be in any form.

The author has further agreed that SFU may keep more than one copy of the Work for purposes of back-up and security; and that SFU may, without changing the content, translate, if technically possible, the Work to any medium or format for the purpose of preserving the Work and facilitating the exercise of SFU’s rights under this licence.

It is understood that copying, publication, or public performance of the Work for commercial purposes shall not be allowed without the author’s written permission.

While granting the above uses to SFU, the author retains copyright ownership and moral rights in the Work, and may deal with the copyright in the Work in any way consistent with the terms of this licence, including the right to change the Work for subsequent purposes, including editing and publishing the Work in whole or in part, and licensing the content to other parties as the author may desire.

The author represents and warrants that he/she has the right to grant the rights contained in this licence and that the Work does not, to the best of the author’s knowledge, infringe upon anyone’s copyright. The author has obtained written copyright permission, where required, for the use of any third-party copyrighted material contained in the Work. The author represents and warrants that the Work is his/her own original work and that he/she has not previously assigned or relinquished the rights conferred in this licence.

Simon Fraser University Library
Burnaby, British Columbia, Canada

revised Fall 2013

Abstract

This thesis introduces a highly sensitive single-axis printed accelerometer based on a flexible paper substrate. The accelerometer is fabricated by cost-effective silver nano ink printing technologies, and consists of a suspended parallel-plate sensing capacitor. By designing the suspension bridge and proof mass structures, the sensitivity to vertical accelerations is optimized based on simulation results. The optimized design with two long ellipse-shaped bridges exhibits a capacitive sensitivity of 20 fF/g at z-axis acceleration of 1-10 g.

A wearable sensing system is proposed which composes of the light-weight flexible accelerometer integrated with a readout circuit. The bandage-type accelerometer system can be conformally attached to various positions on human body for motion detection as well as obtaining vital signs such as human pulse and respiratory rate. Thus, these features allow unobtrusive continuous monitoring of various vital signs and physical activities and acting as a multifunctional sensor in health monitoring system.

Keywords: Paper accelerometer; Modeling and simulation; Printing technology; Silver nano ink; Motion detection; Wearable sensing

Dedication

To my Parents

Acknowledgements

First of all, I would like to give my best acknowledgement to my senior supervisor Dr. Woo Soo Kim. Under his supervision, I have learnt a lot about efficient management and execution of my work. Moreover, he always encourages me to think big and try my ideas even if they do not sound that practicable initially. Great thanks for his remarkable help to me!

Second of all, I deeply appreciate that fellows in *Stretchable Devices Lab* are firmly supporting me in terms of study, work and life all the time. In particular, senior fellow Jiseok Kim is such a nice friend. He contributed so much to my research, and is willing to spare time from his doctoral study to discuss with me whenever I was stuck somewhere. Also, I acknowledge those friends in other labs who are generous to let me use experimental equipment and provide me assistance in different areas of knowledge and technology. In addition, I would like to thank my roommates Hanbo and Rouzbeh for their concern and kindness in daily life.

Last but most importantly, my deeply loved parents are like the brightest stars in the sky, who rejoice and inspire me to move forward when I am walking alone in the darkness. Forever love to my father and mother!

Table of Contents

Approval.....	ii
Partial Copyright Licence.....	iii
Abstract.....	iv
Dedication.....	v
Acknowledgements.....	vi
Table of Contents.....	vii
List of Tables.....	ix
List of Figures.....	x
List of Acronyms.....	xii
Chapter 1. Introduction.....	1
1.1. Flexible electronics.....	1
1.1.1. Overview.....	1
1.1.2. Conductive nanomaterials for flexible electronics.....	2
1.1.2.1 Silver nanowires.....	2
1.1.2.2 Carbon nanotubes.....	4
1.1.2.3 Graphene.....	5
1.1.2.4 Silver nanoparticles.....	6
1.1.3. Patterning technology for flexible electronics.....	7
1.1.3.1 Overview.....	7
1.1.3.2 Printing Technology.....	8
1.2. Accelerometers.....	13
1.2.1. MEMS-based accelerometers.....	13
1.2.2. Applications of accelerometers.....	16
1.3. Vital sign monitoring.....	17
1.4. Motivation of flexible printed accelerometer.....	18
1.4.1. Thesis outline.....	19
Chapter 2. Design of Flexible Capacitive Accelerometers.....	21
2.1. Introduction.....	21
2.2. Mechanical structures and design.....	21
2.2.1. Sensor structure.....	21
2.2.2. Design considerations.....	23
2.3. Modeling and selection of accelerometers.....	25
2.3.1. The choice of variables.....	25
2.3.2. Modeling and simulation results.....	27
Chapter 3. Fabrication and Characterization of Membrane-based Paper Accelerometers.....	36
3.1. Introduction.....	36
3.2. Fabrication of accelerometers.....	37
3.2.1. Patterning of membranes.....	38
3.2.2. Preparation of thin-film silver electrodes.....	39
3.2.3. Sensor assembly.....	40

3.3. Characterization of accelerometers	41
3.3.1. Optimal working frequency range	41
3.3.1.1 Analytical calculations	42
3.3.1.2 Experiments and results	43
3.3.2. Vibrational sensitivity	47
Chapter 4. Integrated Accelerometer System for Biomedical Sensing Applications	51
4.1. Introduction.....	51
4.2. Integration with readout circuit	52
4.2.1. Circuit design.....	52
4.2.2. System validation	54
4.3. Comparison the paper-based sensor with a commercial silicon-based MEMS sensor	56
4.4. Potential biomedical applications	57
4.4.1. Motion detection	57
4.4.2. Pulse measurement.....	58
4.4.3. Heart rate and respiratory rate	59
4.5. Conclusion.....	59
Chapter 5. Conclusions and Future Work.....	60
5.1. Conclusions.....	60
5.2. Future work	61
References	62
Appendix A. Contributions to the Project during Master Thesis	69

List of Tables

<i>Table 2-1 Summarized results for samples with only 2 bridges</i>	<i>31</i>
<i>Table 3-1 Dimensions of three devices.....</i>	<i>41</i>
<i>Table 3-2 Mechanical parameters for accelerometers in two sizes.....</i>	<i>47</i>
<i>Table 4-1 Comparison of specifications of a commercial single-axis silicon-based MEMS accelerometer (Analog Devices ADXL001) and our paper- based printed accelerometer.....</i>	<i>57</i>

List of Figures

Figure 1-1	SEM image of the AgNW film on Si substrate. [14].....	3
Figure 1-2	Different types of carbon nanotubes.	4
Figure 1-3	Diagram of ideal honeycomb structure of graphene.	5
Figure 1-4	TEM images of decanoic acid (C10) capped silver nanoparticles. [38].....	7
Figure 1-5	Mechanism of flexographic printing (a) and offset-gravure printing (b). [45]	9
Figure 1-6	Typical μ CP process steps for depositing metal pattern on a glass substrate [45].....	10
Figure 1-7	Procedures of nanoparticle-based NIL: (i) fix a clean flexible substrate covered by an insulation layer onto a rigid substrate and dispense nanoparticle solution (inset is the schematics of SAM protected AuNPs); (ii) nano-imprinting with PDMS stamp under 40 kPa and 80°C; (iii) annealing of nanoparticles; (iv) peeling flexible substrate off from rigid substrate. [47]	11
Figure 1-8	Schematic representation of mechanism of ink-jet printing.	12
Figure 1-9	Throughput vs. fine pitch comparison for various printing methods. [45].....	12
Figure 1-10	Schematic of a typical accelerometer.	13
Figure 1-11	Fabrication process of a Si micro-accelerometer. [57].....	14
Figure 1-12	Schematic of a piezoelectric accelerometer. [61].....	15
Figure 1-13	Schematic of a piezo-resistive accelerometer. [64].....	15
Figure 1-14	Prototype MEMS capacitive accelerometer architecture. [65].....	16
Figure 1-15	Left: The wearable vital signs monitor worn at the ear. Center: Front side and back side of the monitor. Right: PC interface. [84]	18
Figure 2-1	Schematic of the capacitive membrane-based accelerometer: (a) top view and (b) cross-sectional view.	22
Figure 2-2	Diagram of top membrane under vertical acceleration.....	23
Figure 2-3	The movement of proof mass under pressure load or vertical acceleration.....	26
Figure 2-4	(a-f) Displacement simulation with 20 Pa loading depending on different radius of proof mass, different shapes and numbers of bridge in top membrane	30
Figure 2-5	Summarized displacement simulation results for samples with different shapes and numbers of bridge. [93]	32

Figure 2-6	Displacement simulation of circular proof mass with 20 Pa pressure load with different shapes of bridge in top membrane	34
Figure 3-1	Fabrication process flow of accelerometers.....	38
Figure 3-2	Images of laser-cut paper membranes: (a) top membrane, (b) spacer frame, (c) bottom membrane.	39
Figure 3-3	Schematic illustration of spraying of silver nano ink on top and bottom membranes. [93]	39
Figure 3-4	Image of assembled device. [93].....	40
Figure 3-5	Schematic diagram of the experimental set-up for vibration testing.	44
Figure 3-6	Photographs of accelerometers connected to LCR meter on shaker table.	45
Figure 3-7	Capacitance changes of two accelerometers with different bridges in response to sweeping frequency from 10 Hz to 180 Hz.....	46
Figure 3-8	Capacitance changes of two accelerometers with different sizes in response to sweeping frequency from 10 Hz to 180 Hz. [93].....	46
Figure 3-9	Capacitance response of three accelerometers over a range of 1–10 g acceleration. [93].....	49
Figure 4-1	(a) Schematic diagrams of accelerometer (left) and readout circuit design (right); (b) Fundamental experimental setup that printed accelerometer is connected to readout circuit on breadboard via magnet wires.....	53
Figure 4-2	(a) Experimental setup of pressing test. (b) Sensor response during repeated pressing and releasing. Green: slight press and quick release; Magenta: press the proof mass to the same level, maintain for 5s and then slow release; Blue: press the proof mass to a relatively high level and quick release. Inset is experimental setup of pressing test.	55
Figure 4-3	Schematics of the working principle of motion detection by the accelerometer (top electrode deforms when moving up or down) and the concept of wireless monitoring.	58

List of Acronyms

BCG	Ballistocardiogram
BPM	Beats Per Minute
CNT	Carbon Nanotubes
DC	Direct Current
ECG	Electrocardiography
MEMS	Micro Electro-Mechanical Systems
MWCNT	Multi-walled Carbon Nanotubes
NIL	Nanoimprint Lithography
NP	Nanoparticles
NW	Nanowires
PDMS	Polydimethylsiloxane
PET	Poly(ethylene terephthalate)
PPG	Photoplethysmogram
PU	Polyurethane
PVP	Poly(vinyl pyrrolidone)
R2R	Roll to Roll
RFID	Radio Frequency Identification
SEM	Scanning Electron Microscope
SWCNT	Single-walled Carbon Nanotubes
TEM	Transmission Electron Microscopy
UV	Ultraviolet
μCP	Microcontact Printing

Chapter 1.

Introduction

1.1. Flexible electronics

1.1.1. Overview

This study focuses on developing a disposable, wearable and light-weight accelerometer for biomedical sensing. Such biomedical sensor should be flexible, conformal to human skin, low cost, environment-friendly and easy to use, and also demonstrate high accuracy when detecting biomedical signals including heart rate and human motion. At the start of this thesis, we present a literature review of novel flexible electronics technology which is employed to create our proposed accelerometer.

Flexible electronics is a technology that assembles electronic circuits on flexible substrates, such as paper, polyester films, and polyimide. In recent years, an emerging class of flexible electronics have surpassed their rigid substrate counterparts due to unique features of these being lighter, conformably shaped, more rugged, less expensive and large-area manufacturing compatible [1].

Numerous demonstrations of flexible electronics promise the availability of portable, lightweight, robust and low cost electronics in the near future. The rapid advancement of flexible electronics is fueled by the evolving advances of nanomaterials with a wide range of novel applications in displays [2], RFID tags [3], thin-film transistors [4], sensors [5], antennas [6], photovoltaics [7], light-emitting diodes [8], electronic paper [9] and a wealth of potential applications.

Nanotechnology offers prominent features like solution processability, low processing temperature and tunability in performance, which makes it highly suitable for

flexible electronics manufacturing. Various kinds of conductive nanomaterials including one-dimensional nanowires [6], two-dimensional nanotubes [4], graphene [7] and zero-dimensional nanoparticles [3] has been key to the research success in this blossoming field over the last decade. In terms of electrical conductivity, metallic nanomaterials, especially Ag and Cu, possess the best values among the different types of conductive nanomaterials. Nevertheless, carbon-based nanomaterials possess certain specific properties which meet requirements for specific applications. Details about those important factors in flexible electronics will be summarized in what follows.

1.1.2. Conductive nanomaterials for flexible electronics

To work as electrodes used in flexible sensors for biomedical applications, ideally conductive materials must demonstrate high electrical conductivity and at least intermediate flexibility. Also, the fabrication cost should be low for mass production. Nevertheless, transparency is not a requirement for most sensors.

1.1.2.1 Silver nanowires

As one of the most conductive nanomaterials, silver nanowires (Ag NWs) have attracted a lot of attention from researchers around the globe over last several years [10, 11]. Nanowires are structures that have a diameter of tens of nanometers or less and an unconstrained length. Figure 1.1 shows a SEM image of Ag NWs on Si substrate. Owing to their one-dimensional high-aspect-ratio morphology, Ag NWs possess unique properties like high DC conductivity and optical transmittance [12] for applications of transparent and flexible electrodes. In addition, nanowire antennas show a superior high-frequency response [13].

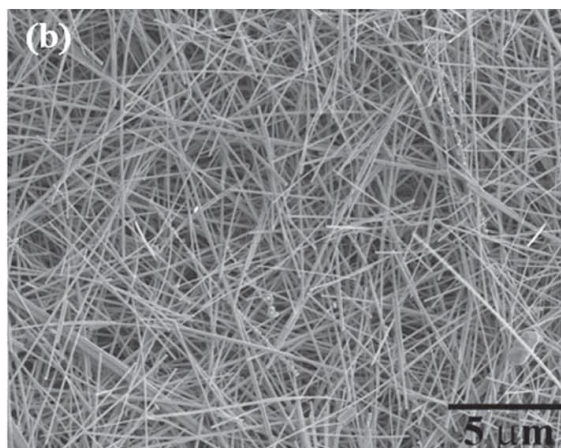


Figure 1-1 SEM image of the AgNW film on Si substrate. [14]

A common synthesis method for Ag NWs is the reduction of silver nitrate in the presence of poly(vinyl pyrrolidone) (PVP) in ethylene glycol [15]. Due to the PVP coating on the surface, the junction resistance is typically high, $\sim 1 \text{ G}\Omega$, and limits the overall conductance of the network. Thus, various methods such as electrochemical annealing and rapid thermal annealing have been exploited to decrease the junction resistance [16]. For instance, sheet resistance decreases notably (from $>1000 \text{ }\Omega/\text{sq}$ to $100\Omega/\text{sq}$) upon heating at $200 \text{ }^\circ\text{C}$ for 20 minutes, because of the fusion of the Ag-Ag junction through the insulating PVP layer [17].

Solution-processed Ag NW electrodes could demonstrate transmittances greater than 85% at sheet resistances less than $20 \text{ }\Omega/\text{sq}$ and electromechanically robustness (no change in resistance after being bent more than 1000 cycles) [12].

However, there are some challenging issues with silver nanowires that limit their applications in flexible electronics. A highly non-uniform topography with Ag NW electrodes can cause shorting through other layers, especially when Ag NWs are used as lower electrodes in devices like solar cells [18]. Additionally, most flexible substrates are not resistant to relatively high annealing temperature ($\sim 200 \text{ }^\circ\text{C}$) which is needed for higher conductance of Ag NW electrodes.

1.1.2.2 Carbon nanotubes

Carbon nanotubes (CNTs), carbon-based nanomaterials that have cylindrical nanostructures with length-to-diameter ratio of up to 132,000,000:1, are promising candidates as conductive materials for flexible electronics. Figure 1.2 illustrates different types of carbon nanotubes.

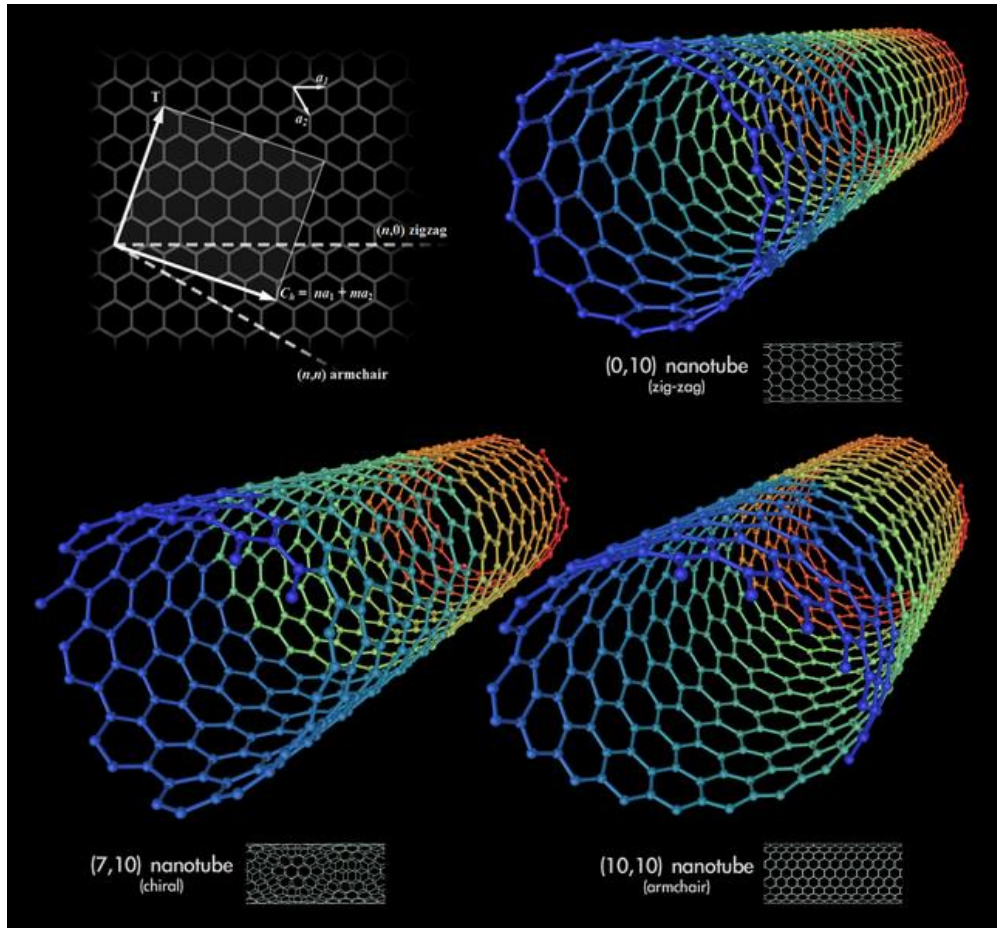


Figure 1-2 Different types of carbon nanotubes.

There are two categories of carbon nanotubes, multi-walled carbon nanotubes (MWCNTs) and single-walled carbon nanotubes (SWCNTs). Depending on their chirality and diameter, CNTs can be either semi-conducting, metallic or semi-metallic.

To produce highly conductive, transparent, and flexible films of CNTs, two main methods are commonly used: (1) superaligned films of CNTs drawn from vertically

grown CNT forests via the “dry-drawing” technique [19], and (2) films of CNTs deposited onto or embedded in flexible or elastomeric substrates such as PET, Polydimethylsiloxane (PDMS) and Ecoflex [20, 21]. Simple solution deposition methods such as spray coating and slot dye coating are applied to the deposition of CNTs. Lipomi *et al.* [22] reported transparent, conducting spray-deposited films of SWCNTs that obtain values of $R_s=328 \Omega/\text{sq}$ and $T=79\%$ and accommodate strains of up to 150% with conductivities of 2200 S/cm.

CNTs’ unique nanostructure offers many features required in transparent electrodes, such as their high intrinsic conductivity, flexibility, solution processability, and the potential for production at low cost. To date, CNTs have been applied to a raft of flexible or stretchable devices such as pressure and strain sensors [23], chemical or biological sensors [24], touch screens [25], displays [26], solar cells and super capacitors [27, 28]. However, CNTs are still faced with the issues of the high cost and scalability in the means of the separation of metallic CNTs from semiconducting CNTs.

1.1.2.3 Graphene

Graphene is another allotrope of carbon which is a one-atom thick planar sheet with honeycomb lattice arrangement as shown in Figure 1.3. It is rapidly emerging as conducting carbon-based nanomaterials for transparent electrodes applications. A lot of strategies to prepare large-scale graphene have been developed, including self-assembly of reduced graphene oxide and graphite crystal [29, 30], epitaxial growth on silicon carbide [31] and ruthenium [32] and direct synthesis of graphene films using chemical vapour deposition [33].

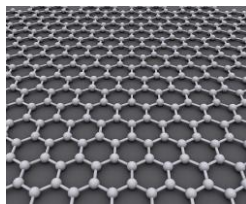


Figure 1-3 Diagram of ideal honeycomb structure of graphene.

In contrast to CNTs, graphene possesses better conductivity, higher transparency, and some unique chemical and physical properties. For instance, Bae *et al.* [34] demonstrated large area doped graphene sheets using a roll-to-roll transfer process which shows an R_s of $30\Omega/\text{sq}$ at a T of 90%. In addition, graphene is chemically the most reactive form of carbon, owing to the high surface area and highest ratio of edgy carbons in comparison with similar carbon-based materials [35]. As a result, Graphene is an ideal candidate as thin-film electrodes in chemical and temperature sensors. Nevertheless, because of the tightly controlled laborious fabrication processes, it is difficult to produce high quality graphene films in large quantities for industrial applications of flexible electronics.

1.1.2.4 Silver nanoparticles

In nanotechnology, nanoparticles are defined as bits of a material in which all three dimensions of the object are within the nanoscale. Nobel metallic nanoparticles, especially silver nanoparticles, have been successfully explored as low-temperature, high-conductivity printable materials as electrodes, conductive lines, tracks, and pixel pads in enabling low-cost electronics [36, 37].

Silver nanoparticles are formulated by being stabilized with a thin organic layer like alkylamine [37] on it. The surfactants and their chain lengths play a major role in tailoring properties like dispersion and stability in a solvent, and sintering temperature at which deposited nanoparticles become conductive. Ankireddy *et al.* [38] recently reported that micro-electrodes printed with silver nanoparticles capped by short chain carboxylic acids exhibit a conductivity of 10 to 87% of the bulk silver conductivity with the sintering temperature as low as 130 to 250 °C. A TEM image of resulting AgNPs is presented in Figure 1.4.

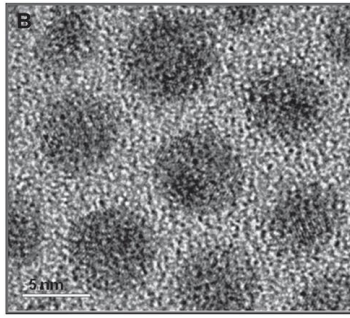


Figure 1-4 TEM images of decanoic acid (C10) capped silver nanoparticles. [38]

Various nanomaterials including silver nanowires, graphene, carbon nanotubes and silver nanoparticles have been introduced as electrodes for flexible electronics. Among all these conductive materials, metallic nanoparticles have been most commonly used due to their high conductivity and other features such as thermal stability, and chemical inertness [36, 39].

1.1.3. Patterning technology for flexible electronics

1.1.3.1 Overview

Flexible electronics manufacturing mainly includes four steps: preparation of materials, deposition, patterning, and encapsulation. As a crucial step in fabrication, patterning technology has greatly stridden from conventional lithography to novel printing techniques. Four major factors have to be considered containing cost, throughput, achievable feature size, and compatibility with flexible substrates.

Optical lithography and other conventional techniques are well-established for fabricating microelectronic devices. Regardless of their high resolution, they are not quite suitable for flexible electronics because of their complex, expensive, time-consuming processes and requiring resists, solvents, developers, and high temperature incompatible with flexible substrates in processing [40].

In comparison, printing technology is a much simpler, cost-effective and high-throughput fabrication method, typically uses common printing equipment such as gravure and inkjet, and may not require vacuum or other harsh manufacturing conditions. Also, printing methods use device materials efficiently by implementing depositing and

patterning materials in one single step. Thanks to these exceptional characteristics, printing techniques have attracted a lot of attention for fabrication of flexible electronics.

For low-cost flexible sensors for biomedical sensing, this thesis is targeting a printing method that can produce electronic devices with high speed and low cost. In addition, low printing resolution is acceptable.

1.1.3.2 Printing Technology

Two main types of printing techniques have been developed: (1) roll-to-roll based approaches, such as gravure, offset and flexographic printing; (1) sheet-based approaches, such as screen-printing and inkjet printing. Besides, there are other methods with similarities to printing, among which micro-contact printing (μ CP) and nanoimprint lithography are of interest. All techniques have their unique features and drawbacks, and modifications of the conventional methods are required in order to print fine patterns for electronics.

Flexo, offset, and gravure printing have been widely used for high-volume R2R mass production [41-44]. Figure 1.5 shows the mechanism of flexo and gravure printing techniques. The print patterns are typically created by chemical etching or photolithography, and high print resolution ($\sim 45 \mu\text{m}$) can be achieved [45]. In R2R processes, the ink is first transferred to a cylinder with print pattern then printed onto a flexible substrate at a high pressure. The rather high print pressure limits the use of those techniques to applications where it may destroy previously printed soft layers on the substrate. Other factors to take into consideration are the limited solvent compatibility of the flexible plates in flexo printing and the presence of water in offset printing [46].

Microcontact printing (soft lithography) is a fine pattern printing technology that can be applied to microstructure formation with a feature size of approximately 100 nm [45]. The μ CP method uses a PDMS stamp to form patterns of self-assembled monolayers of ink that attracts metallic elements such as Au or Ag on the surface of a substrate. A typical process flow of μ CP is illustrated in Figure 1.6. Therefore, it is compatible with high-throughput batch or R2R technology. In addition, it can produce

excellent resolution as small as 60 nm at rates of centimeters per second, but have difficulty in patterning multiple layers [47].

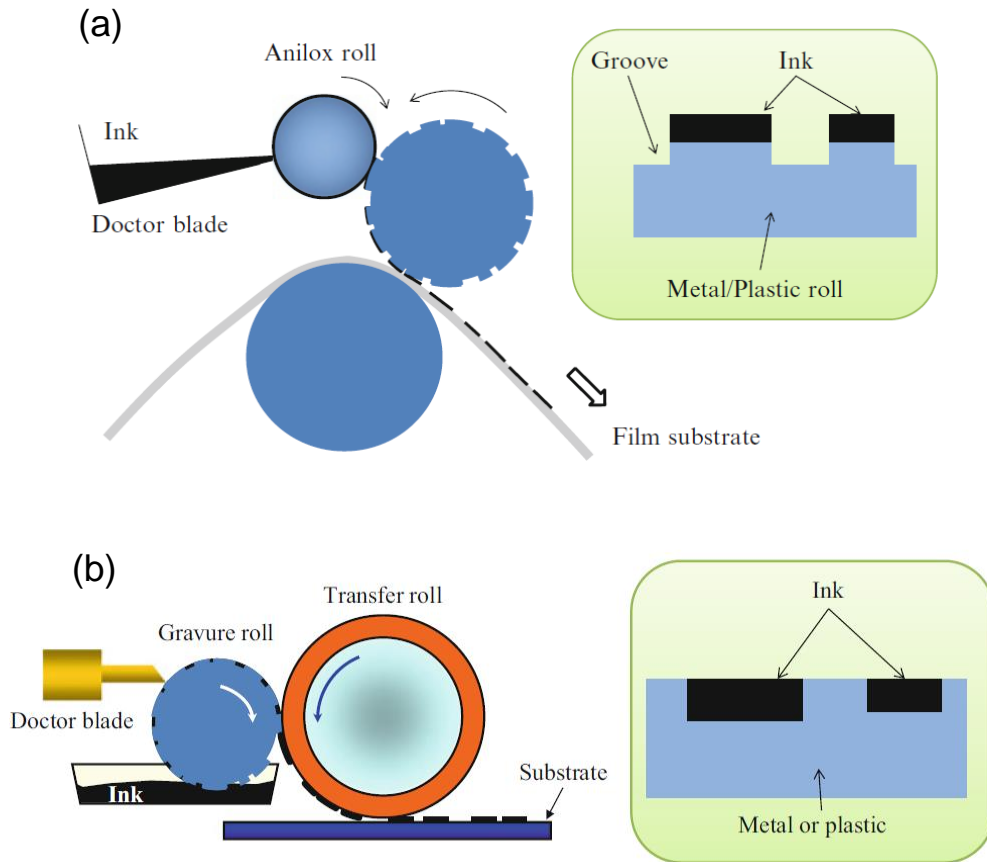


Figure 1-5 Mechanism of flexographic printing (a) and offset-gravure printing (b). [45]

Nanoimprint lithography (NIL) is another fine patterning method that is able to provide submicron structure formation. Conventionally, NIL refers to the pressure-induced transfer of a topographic pattern from a mold or stamp into a thermoplastic polymer like PMMA and then acting as a mask for metal film etching or metal lift-off process. However, flexible substrates cannot resist the high temperature and pressure during the imprinting process.

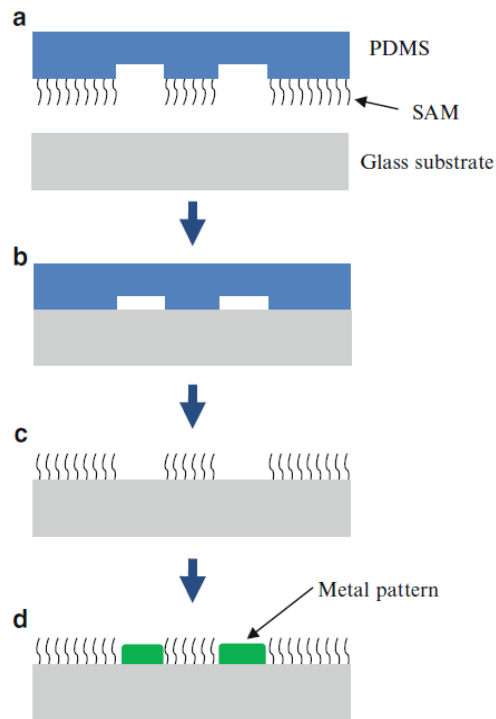


Figure 1-6 Typical μ CP process steps for depositing metal pattern on a glass substrate [45]

Alternatively, Park *et al.* [47] announced metal nanopatterning on flexible substrates via a direct nanoimprinting process of metallic nanoparticles. This process involves a direct metal patterning in ultrafine nanoscale dimensions with very low pressure and temperature requirements, and process simplicity. Process steps of direct nanoimprinting of metallic nanoparticles on flexible substrates are shown in figure 1.7. For nanopatterning using NIL, some issues like incomplete nanopattern replication and non-uniform pattern height are still to be resolved. Additionally, the useful lifetime of the mold presents another challenge because of pressure-induced stress and wear on nanoimprint molds during heating and cooling cycles [48].

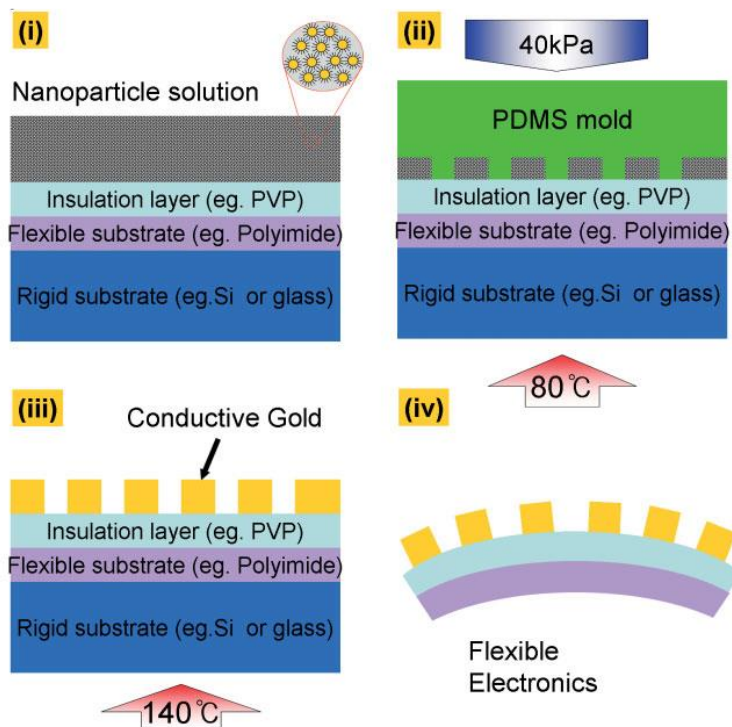


Figure 1-7 Procedures of nanoparticle-based NIL: (i) fix a clean flexible substrate covered by an insulation layer onto a rigid substrate and dispense nanoparticle solution (inset is the schematics of SAM protected AuNPs); (ii) nano-imprinting with PDMS stamp under 40 kPa and 80 °C; (iii) annealing of nanoparticles; (iv) peeling flexible substrate off from rigid substrate. [47]

Inkjet printing is a promising digital lithography method for directly writing solution-processable functional materials at room temperature. The process essentially involves the ejection of a fixed quantity of ink drop generated either thermally or piezo-electrically through a nozzle, drop falling, and spreading on the substrate as shown in Figure 1.8.

As a noncontact printing process, the inkjet printing has several advantages including the low-cost easily changeable digital print patterns, excellent compatibility with organic and inorganic materials and low material consumption. However, although it is totally R2R compatible, inkjet printing has a limited printing speed, and faces with several challenges in terms of ink formulation, driving mode, substrate selection, and control of solvent evaporation [49].

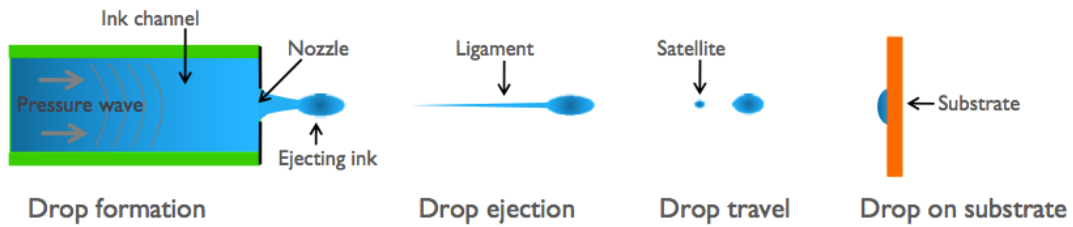


Figure 1-8 Schematic representation of mechanism of ink-jet printing.

Spray coating, an alternative directly writing method, is a technique that involves forcing the printing ink in a carrier gas through a nozzle. This cost effective method allows a wide range of ink viscosities and deposition at room temperature without specialized equipment [50, 51]. These characteristics and its R2R compatibility make it useful for rapid prototyping.

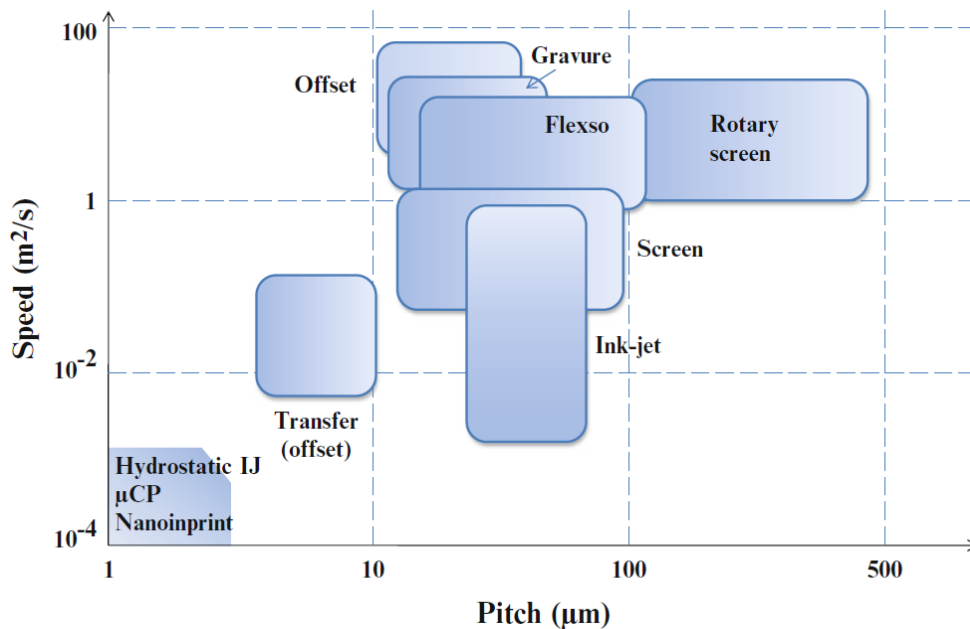


Figure 1-9 Throughput vs. fine pitch comparison for various printing methods. [45]

There is not a single printing technique that is perfectly suitable for printing electronics. Various printing methods exhibit different printing speeds and pitch resolution as shown in Figure 1.9. One must make a suitable choice of which printing techniques to use regarding the requirements on the lateral resolution, printing speed, printed thickness, homogeneity, materials and ink properties.

Concerning all those requirements, the selected spraying method would be a great choice as printing method in manufacturing our biomedical sensors because of their fast speed, homogeneous deposition in wide area, compatibility of metallic nanomaterials with paper substrates, and relatively low cost.

1.2. Accelerometers

1.2.1. MEMS-based accelerometers

An accelerometer is a mechanical sensor that measures linear acceleration along one or several axes. Typically, an accelerometer works as a system consisting of a damped mass on a spring as illustrated in Figure 1.10. In this system, the mass used in accelerometers is often called the seismic-mass or proof-mass. The dynamic behaviour of this classical second order mechanical system in the z direction can be mathematically represented by

$$\begin{aligned}
 m\ddot{x} + F_{damping} + F_{spring} &= 0 \\
 m\ddot{x} + c\dot{x} + kx &= 0
 \end{aligned}
 \tag{1.1}$$

where m is the effective mass, c is the damping constant, x is relative movement of the proof-mass with respect to frame, and k is the spring constant.

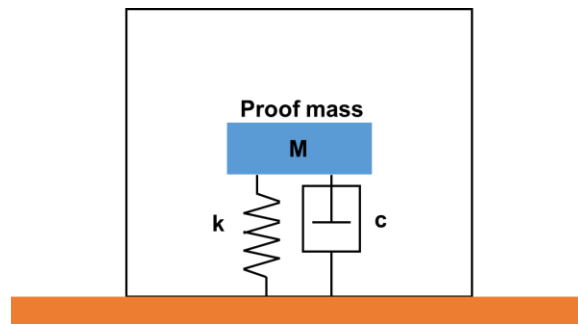


Figure 1-10 Schematic of a typical accelerometer.

Modern accelerometers are often manufactured by micro electro-mechanical systems (MEMS) technology [52-54]. MEMS technology involves small systems with

both mechanical devices and electrical components, mostly fabricated from silicon and using techniques derived from the microelectronics industry [55]. Those include basic processes: photolithography, anodic bonding, isotropic and anisotropic etching, and various thin film deposition methods.

For MEMS-based accelerometers, the mass-spring structure is realized in silicon substrates using surface or bulk micromachining processes. For example, the fabrication process of a Si micro-accelerometer is illustrated schematically in Figure 1.11. MEMS devices typically hold advantages including small-size (in the range of 300 nm to 300 μm), light-weight, low-cost, high-performance and low power consumption against their large-size counterparts [56].

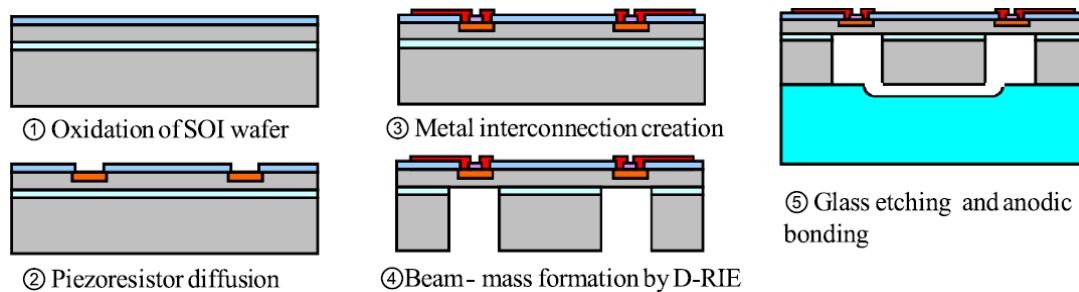


Figure 1-11 Fabrication process of a Si micro-accelerometer. [57]

Based on the position sensing mechanism, accelerometers can be classified as three main types of sensors: piezoelectric, piezo-resistive and capacitive accelerometers. Detection of acceleration is accomplished either by direct observation of the displacement of the proof mass (mostly capacitive electrodes), or by detection of the deformation of the support (piezo-resistive or piezoelectric sensors).

Piezoelectric accelerometers employ the piezoelectric effect of ceramic materials (e.g. lead zirconate titanate) or single crystals (e.g. quartz) [58, 59]. In Figure 1.12, a typical configuration of a piezoelectric accelerometer is presented. When a physical force is exerted on the accelerometer, the proof mass imposes a force on the piezoelectric material resulting an electrical voltage output that is proportional to applied acceleration. Some of its advantages include very high shock survival (up to 100,000 g) and high frequency range (10 kHz) [60]. Nevertheless, these accelerometers cannot

directly measure DC and very low frequency accelerations due to the nature of piezoelectric materials which respond to changes in stress.

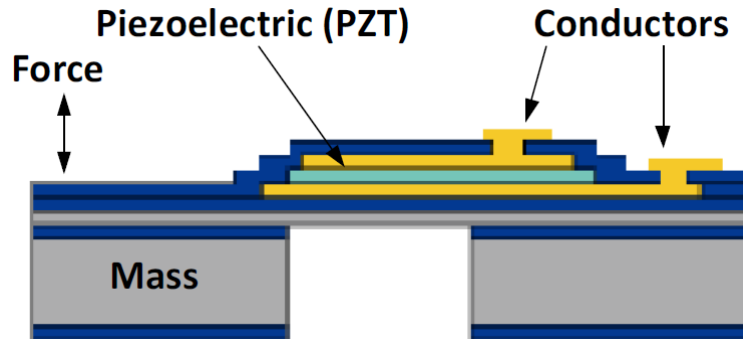


Figure 1-12 Schematic of a piezoelectric accelerometer. [61]

Piezo-resistive accelerometers use piezo-resistors in place of the piezoelectric materials as shown in Figure 1.13, and the force exerted by the proof mass changes the resistance of piezo-resistors. Piezo-resistive accelerometers have the advantage over piezoelectric accelerometers in that they can measure accelerations down to zero Hz. Besides, piezo-resistive accelerometers can also survive high shock conditions, and tend to have a simple interface [62]. However, they have some drawbacks in terms of their sensitivity [63], temperature dependence, and high power consumption.

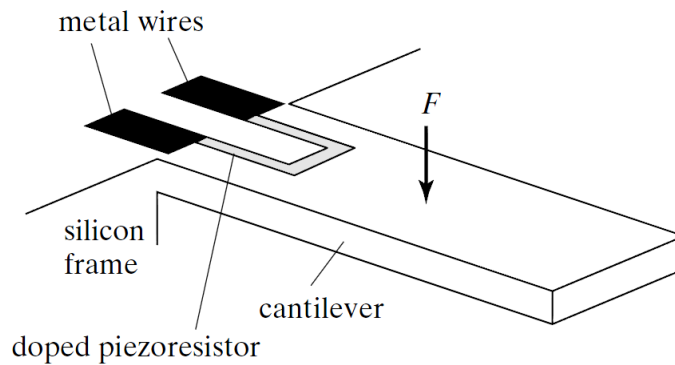


Figure 1-13 Schematic of a piezo-resistive accelerometer. [64]

Capacitive accelerometers measure the displacement of the proof mass via capacitive electrodes. As the proof mass moves towards or away from the electrodes, a differential change in the capacitance is detected which can be converted to a voltage

output. A schematic diagram of MEMS capacitive accelerometer is illustrated in Figure 1.14. In contrast to other two types of sensors, capacitive sensors provide a large output signal, good steady-state response and better sensitivity due to low noise performance. Since the dielectric material is typically air, they can work over a wide temperature range and have minimal temperature dependence [62]. Moreover, capacitive accelerometers tend to work over a low frequency range.

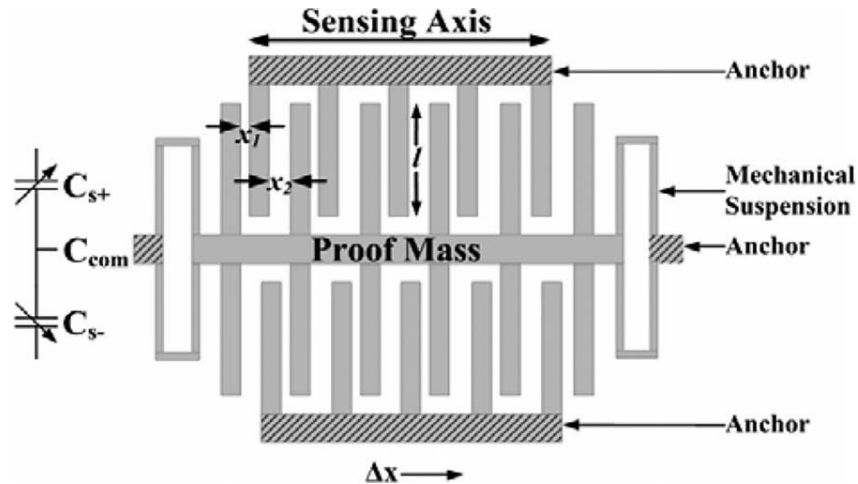


Figure 1-14 *Prototype MEMS capacitive accelerometer architecture. [65]*

1.2.2. Applications of accelerometers

Basically, accelerometers can detect magnitude and direction of the proper acceleration. Derived from this basic idea, an accelerometer is available to sense orientation (because direction of weight changes), gravity, vibration, shock, coordinate acceleration, and falling in a resistive medium. Hence, accelerometers have multiple applications in various fields of industry and science.

First of all, accelerometers are essential components in automotive and consumer electronics applications [66]. Accelerometers can sense the inclination and accelerations of vehicles for airbag deployment, active suspension control, active steering control, anti-lock braking and other safety or control systems requiring accelerometers' high sensitivity to out-of-plane force [67, 68]. In personal electronics devices, accelerometers can be used to detect the orientation of the devices for

adjustment to the display screen [69], input motion for gaming controllers and smart phones, and detect drops for activating protection system [70].

Second, accelerometers are widely used in industry and structural monitoring [71-74]. For machinery health monitoring, accelerometers are used to report the vibration and its changes in time of shafts at the bearings of rotating equipment such as turbines and pumps. For structural health monitoring, accelerometers are integrated to measure the motion and vibration of a structure (e.g. buildings and bridges) that is exposed to dynamic loads for safety and viability assessment.

Lastly, accelerometers play a crucial role in health monitoring and rehabilitation [75-77]. Detection of daily physical activities is commonly achieved by the single use of accelerometers or integration with carry-on electronics like smartphones [78-80]. The profile of daily physical activities is an important factor when assessing the health of a person, especially in the case of cardiovascular diseases [80]. In addition, the continuous monitoring of acceleration could lead to the detection of gait and balance disorders in-time and an effective fall detection alarm for elderly people or patients [81, 82].

1.3. Vital sign monitoring

Vital signs represent measures of various physiological statistics, which are used to assess the most basic body functions of human. Vital signs primarily include pulse rate (or heart rate), respiratory rate, body temperature, and blood pressure, but may also include other signs such as pain. Continuously monitoring of vital signs is essential to monitor the status of patients in situations of treating emergency, outpatient, and long or short-term hospitalized patients. In addition, vital sign monitoring can provide family physician or caregiver data for routine monitoring of cardiovascular diseases (by heart rate), diabetes and hypertension (by blood pressure) at home or other places outside of hospitals [83, 84].

Currently, the commercially available vital signs measurement devices, such as electrocardiogram (ECG) Holter and cuff blood pressure monitor, are still a bit bulky in

terms of their size. The usage of these devices includes skin preparation for ECG measurement as well as tightly wrapping the cuff around the arm, which are often unpleasant and restrictive for patients, especially elderly people [85].

In order to resolve those issues, several research groups have developed portable and cost-effective measurement systems to monitor multiple vital signs for personal health care. Guo *et al.* [85] demonstrated a long-term vital signs monitoring system which can measure various physiological signs. This monitor measures ECG with a chest belt, photoplethysmograms (PPG) with an ear-worn probe, and systolic blood pressure using the pulse-arrival time method.

Winokur *et al.* [84] designed a continuous, wearable and wireless vital signs monitor at the ear in the form factor of a hearing aid. This device can monitor single lead ECG, ballistocardiogram (BCG), and PPG at one location for improved patient compliance. Figure 1.15 shows the entire prototype system anchored to the ear. Still those vital sign monitoring systems are a bit bulky, and need to be improved to become high-fidelity, easy-to-use and minimally obtrusive devices for daily life use.



Figure 1-15 Left: The wearable vital signs monitor worn at the ear. Center: Front side and back side of the monitor. Right: PC interface. [84]

1.4. Motivation of flexible printed accelerometer

MEMS technology is currently growing at a dramatically accelerated rate in the microelectronics industry. Its global market has approached several billions of units in

recent years [55, 86]. Typical MEMS devices, such as accelerometers, have been widely used in automotive industry, consumer electronics, structural health monitoring, and machine health monitoring. In addition to these fields, accelerometers also begin to gain much attention in biomedical applications such as hearing aids [54], wearable sensors including motion detectors [80] and blood pressure sensors [87].

Although MEMS accelerometer is so attractive due to its tiny size, its time-consuming, complex and expensive fabrication processes limit its further advance [88]. Also, these micro machining processes are incompatible with flexible substrates in terms of high processing temperature and corrosive liquid etchants. On the contrary, printing technology is inexpensive, process-effective, fully compatible with flexible substrates, and able to pattern fine micro-scale structures on substrates. Besides, paper, readily available and light-weight, is a new alternative to serve as flexible substrates for MEMS devices with high potential for extremely low cost device fabrication [89, 90]. And some paper-based MEMS devices have shown great performance in recent researches [3, 90, 91].

To combine accelerometers with novel printing technology, this thesis tries to develop a flexible printed accelerometer. In particular, this light-weight flexible accelerometer is an excellent candidate as wearable or attachable sensor for pervasive sensing in e-healthcare systems. We present the high sensitivity of this accelerometer to motion and accelerations over a low frequency range, and its possibility to detect and measure body movement and human pulse by integration with an interface circuit.

1.4.1. Thesis outline

This thesis comprises 5 Chapters. Theoretical background for the understanding of accelerometers and recent research progresses in flexible electronics have been introduced in Chapter 1.

- Chapter 2 introduces a novel structure design for printed single-axis capacitive type accelerometers. Through modeling and simulation, parameters of this configuration are selected to achieve high sensitivity to vertical accelerations.

- Chapter 3 presents an efficient fabrication method using paper substrates and printing technology for fabricating proposed accelerometers. Fabricated accelerometers are tested under sinusoidal vibration with sweeping frequency and different amplitudes to obtain their working frequency range and capacitive sensitivity.
- Chapter 4 demonstrates a well-designed interface circuit to convert capacitance change signal to an easily measurable format like voltage output signal. Such integrated accelerometer system works properly as we expected under a simple pressing test. In terms of sensitivity and other specifications, the performance of our paper-based accelerometer is compared with a commercial silicon-based MEMS accelerometer. This chapter also introduces potential biomedical sensing applications for the flexible paper-based accelerometer system.
- Finally, Chapter 5 gives the conclusions and future research to improve this accelerometer system.

Chapter 2.

Design of Flexible Capacitive Accelerometers

2.1. Introduction

Accelerometers typically use three sensing methods: capacitive, piezo-resistive and piezoelectric. Capacitive accelerometers sense a change in electrical capacitance, with respect to acceleration. A capacitive approach allows several benefits including high sensitivity, low drift, good noise performance, and simplicity when compared to other two methods [92]. Also, since the dielectric material is air, they have minimal temperature dependence and a wide working temperature range [62]. In particular, its performance is superior in the low frequency range, which fits potential applications of flexible accelerometers in biomedical sensing. For those reasons, capacitive sensing is chosen as the sensing method for our accelerometers.

In this work, we develop a flexible accelerometer that employs capacitive sensing. This chapter first introduces the basic design of mechanical structures of capacitive accelerometers, and then presents the selection of parameters settings by modeling and simulation of sensor samples under same working conditions.

2.2. Mechanical structures and design

2.2.1. Sensor structure

Capacitive accelerometers use capacitively coupled surfaces for the sensing of displacement. Typically, three different designs are implemented: parallel plate capacitor, inter-digitated capacitor, and fringing capacitor. In this approach, the capacitive structure

of accelerometers is composed of two parallel membrane electrodes, where the proof mass as the movable plate electrode is in the top membrane and the bottom is the stationary electrode. Two electrodes are separated by a thin insulating layer.

Conceptually, accelerometers behave as a second-order mass-spring-damper system [52]. Figure 2.1 illustrates the top and cross-sectional views of the device structure. Both top (darker blue) and bottom (lighter blue) membranes are defined in a flat round shape plate. In the top membrane, a round shape proof mass is connected to an anchor ring via several suspension beams (bridges). And, the shape of bridges can be any kind, such as straight line, zigzag line and winding line. This design uses the entire proof mass in the mechanical structure also as the movable plate electrode in the capacitive sensing mechanism and each suspension beam as a spring in the damping mechanism.

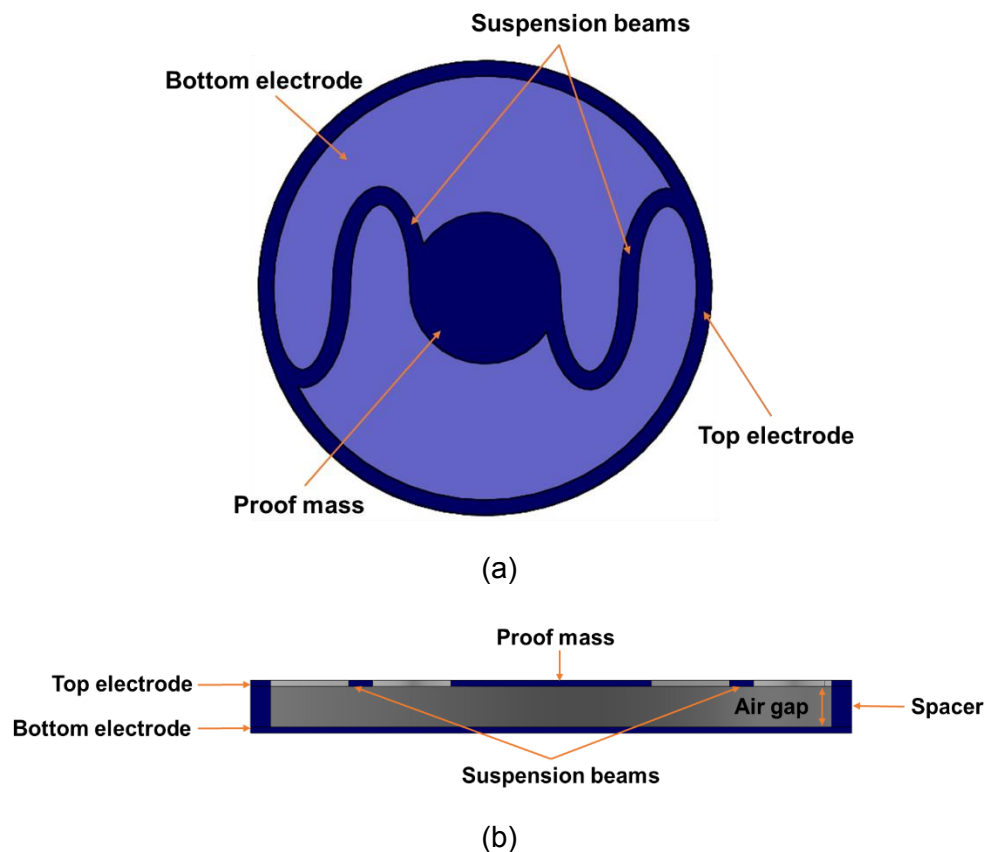


Figure 2-1 Schematic of the capacitive membrane-based accelerometer: (a) top view and (b) cross-sectional view.

2.2.2. Design considerations

The dimensions of the anchor ring are fixed to 14 mm × 14 mm. Inside of the fixed anchor ring, some parameters of proof mass and suspension beams can be selected to obtain a high performance as an accelerometer. At first, we start our approach from theoretical analysis of how the sensor works as a variable capacitor.

Basically, the parallel plate capacitive configuration detects accelerations when the capacitance of the device is altered by varying the gap between the plates. As a result, the capacitance C between two membrane electrodes can be expressed as

$$C = \varepsilon \frac{A}{d}, \quad (2.1)$$

where ε is the permittivity of air, A is the overlapped area and d is the distance between two membranes.

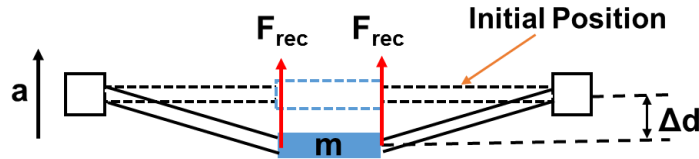


Figure 2-2 Diagram of top membrane under vertical acceleration

As shown in figure 2.2, when subject to an external acceleration (normal to the proof mass) a , the proof mass deflects toward or away from the bottom electrode due to inertial force. Treating the proof mass as a free body and applying Newton's second law, the total force F_{tot} on the body is

$$F_{tot} = ma = nF_{rec} = \rho \pi r^2 t a, \quad (2.2)$$

where m and r are the mass and radius of the proof mass respectively; ρ and t are the density and thickness of the top membrane respectively; n is the number of suspension beams; F_{rec} is the recall force from each suspension beam.

From a mechanical point of view, suspension beams in the top membrane can be considered as cantilever beams. Considering the shape of suspension beams is not

straight, the spring constant of cantilever beams k is given by

$$k = \frac{3EI}{L_{eff}^3}, \quad (2.3)$$

where E , L_{eff} , and w are the Young's modulus, effective length and width of bridges; I is second moment of inertia of beam cross section (rectangle).

And according to the ref.[52], the equivalent flexural rigidity EI of bi-layer silver-paper suspension beams is given by

$$EI = \frac{w \left[(E_p t_p^2)^2 + (E_s t_s^2)^2 + 2E_p E_s t_p t_s (2t_p^2 + 3t_p t_s + 2t_s^2) \right]}{12(E_p t_p + E_s t_s)}, \quad (2.4)$$

where E_p and t_p are Young's modulus and the thickness of the paper membrane, E_s and t_s are Young's modulus and the thickness of silver, w is the width of suspension beams. The width of suspension is defined by the fabrication method, and all the other parameters in these equations are defined by those two materials. As a result, the equivalent flexural rigidity can be considered as a constant in following analysis.

Thus, the recall force F_{rec} is

$$F_{rec} = k\Delta d = \frac{3EI}{L_{eff}^3} \Delta d, \quad (2.5)$$

where Δd is the deflection of beams as well as the displacement of the proof mass. Based on the configuration, electrostatic attraction from the bias voltage and fringing fields induce almost no deflection of proof mass, and can be neglected in the calculation.

From equation (2.2) and (2.5), the displacement of the proof mass is calculated as

$$\Delta d = \frac{\pi \rho r^2 t L_{eff}^3}{3nEI} a, \quad (2.6)$$

Derived from equation (2.1) and (2.5), differentiating C with respect to a , the

capacitance change of the capacitor due to vertical acceleration is expressed as

$$\frac{\delta C}{\delta a} = \frac{\frac{\pi^2 \rho r^4 t L_{eff}^3}{3nEI}}{\left(d_0 - \frac{\pi \rho r^2 t L_{eff}^3}{3nEI} a \right)^2}, \quad (2.7)$$

where d_0 is the initial gap between two plates. Considering much smaller area and displacement of bridges, the value δC is mainly contributed by the capacitance change of proof mass in this equation.

2.3. Modeling and selection of accelerometers

2.3.1. The choice of variables

From equation (2.7), the value $\frac{\delta C}{\delta a}$ represents the device's sensitivity to z-axis acceleration. In order to achieve higher sensitivity, some parameters in the equation can be selected in the device structure. For instance, the number and length of suspension bridges can be changed so as to improve the sensitivity. In our approach, we vary the radius of proof mass and number of bridges, and design different shapes of bridges in order to reach the highest sensitivity. And CAD software Solidworks and engineering simulation software ANSYS® is used to model the structure of top membrane and simulate the movement of center proof mass under accelerations.

Electrodes' thickness, density and young's modulus are already defined by constructing materials (paper) and conducting material (silver). Additionally, other factors like the radius of anchor ring (7 mm), and bridge's width (0.6 mm) are fixed in all samples identically. 3D design of the top membrane structures is drafted and modeled in SolidWorks 2012.

Simulation of the device under vertical accelerations is achieved by applying pressure orthogonal to the proof mass in ANSYS® Workbench 14.5. Through this modeling and simulation, the displacement of proof mass measured under pressure load

can be employed to simulate the displacement of proof mass under accelerations. Figure 2.3 demonstrates the equivalent movement of proof mass under pressure load or acceleration.

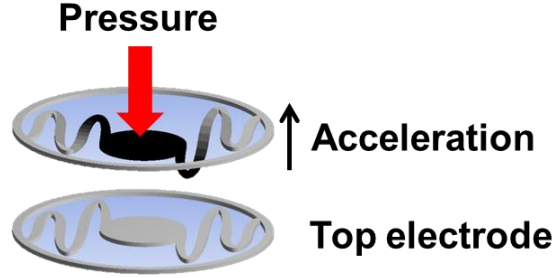


Figure 2-3 The movement of proof mass under pressure load or vertical acceleration

The mechanical equivalence can be explained by mathematical calculations. While the proof mass is loaded with pressure of P , substituting k from equation (2.3), the displacement of proof mass $\Delta d'$ is written as

$$\Delta d' = \frac{F_{rec}'}{nk} = \frac{PA}{nk} = \frac{P\pi r^2}{n \frac{3EI}{L_{eff}^3}} = \frac{\pi \rho r^2 t L_{eff}^3}{3nEI} \frac{P}{\rho t}, \quad (2.8)$$

where F_{rec}' is the total recall force from suspension beams which is equal to the external force provided by the applied pressure.

As the form of equation (2.8) is identical to that of equation (2.6), the acceleration, a , in equation (2.6) is equivalent to $\frac{P}{\rho t}$. Thus, the test conditions that a pressure load of P is applied to the proof mass in ANSYS can simulate conditions that an acceleration of $\frac{P}{\rho t}$ is applied to the device. Larger displacement of proof mass means easier movement of proof mass, hence, higher sensitivity of entire accelerometer from certain external acceleration.

From equation (2.7), we know that larger radius of proof mass (r), smaller

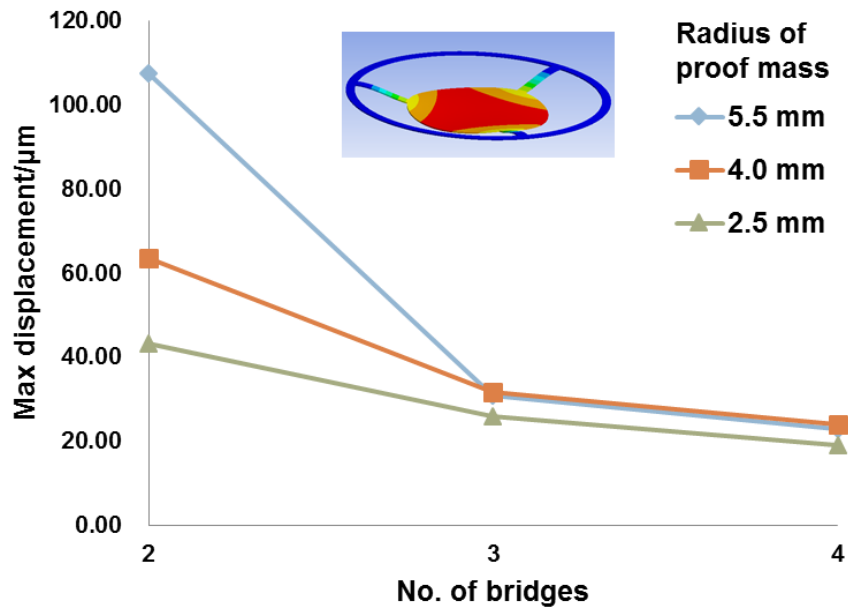
number (n) and larger effective length (L_{eff}) of bridges are required for higher sensitivity. However, larger r results in smaller L_{eff} for the top membrane with certain shape of bridges. Therefore, we simulate the test conditions that an acceleration of $\frac{P}{\rho t}$ is applied to the samples with varying r , L_{eff} , and n and measure the displacement of center proof mass so as to find a balance point between r and L_{eff} .

In order to compare different bridge shape's length dependency, five different bridge shapes are chosen representatively such as straight line, zigzag line, round-shape, and ellipse. And, for samples with same shape of bridges, the radius of proof mass changes among 2.5 mm, 4 mm and 5.5 mm. Also, different patterns with 2, 3 or 4 bridges are tested under same test conditions.

2.3.2. Modeling and simulation results

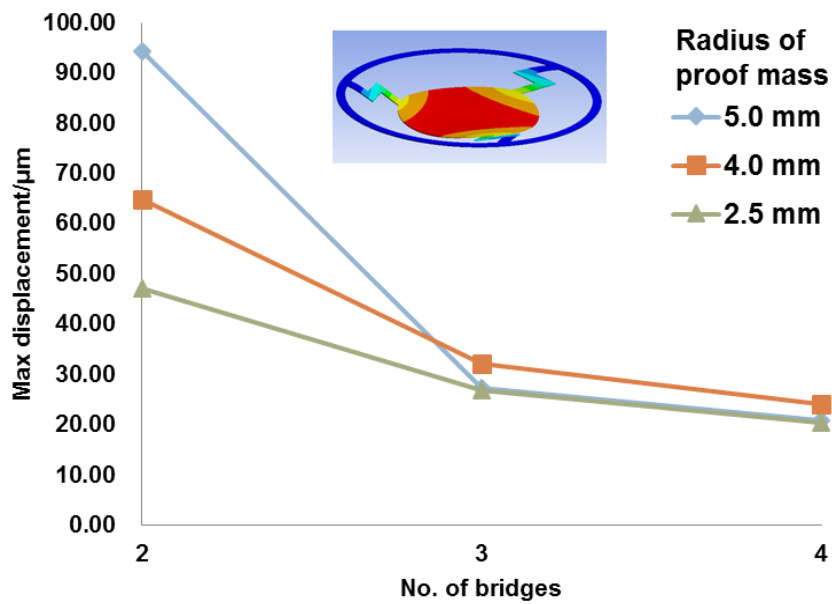
By exploiting the function of *static structural*, we implement the modeling and simulation of different samples in ANSYS. First, the geometry of the device is imported and generated from the drawing created in Solidworks. Paper is selected as the constructing material. Then, in simulation section, we apply a fixed support to the anchor ring and a pressure load of 20 Pa to the proof mass uniformly. Finally, the displacement of proof mass and suspension beams is solved for each sample separately. The simulation results and illustrations of bridge shapes are shown in Figure 2.4.

Shape #1

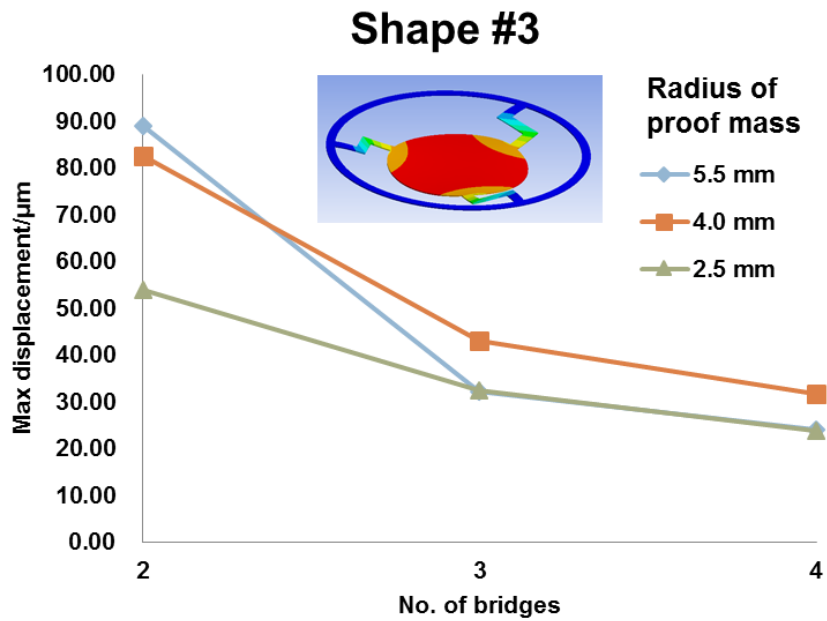


(a) Straight line

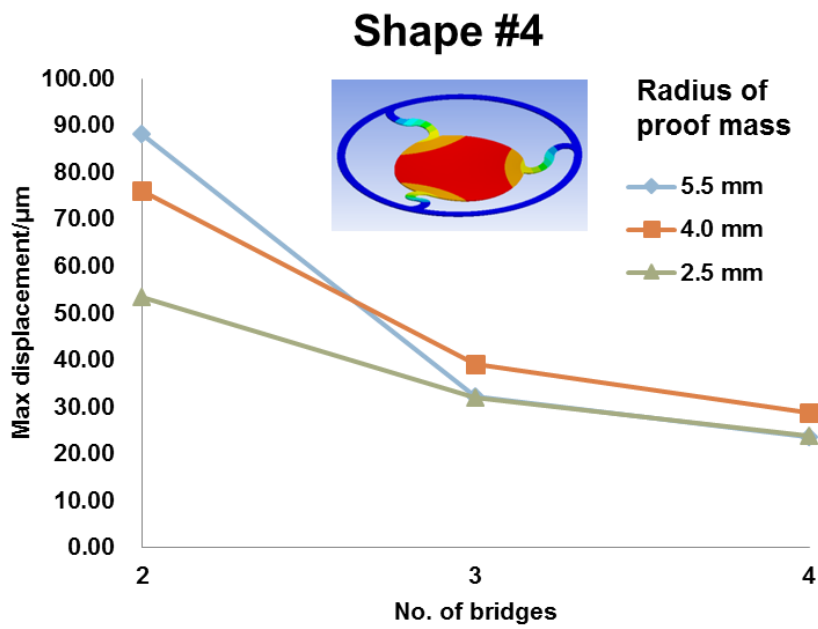
Shape #2



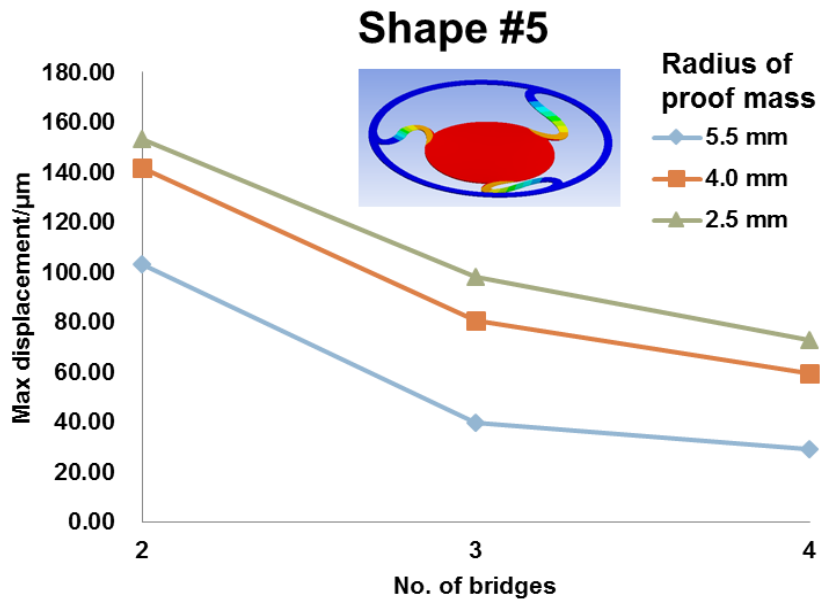
(b) Zigzag line with a corner angle of 60°



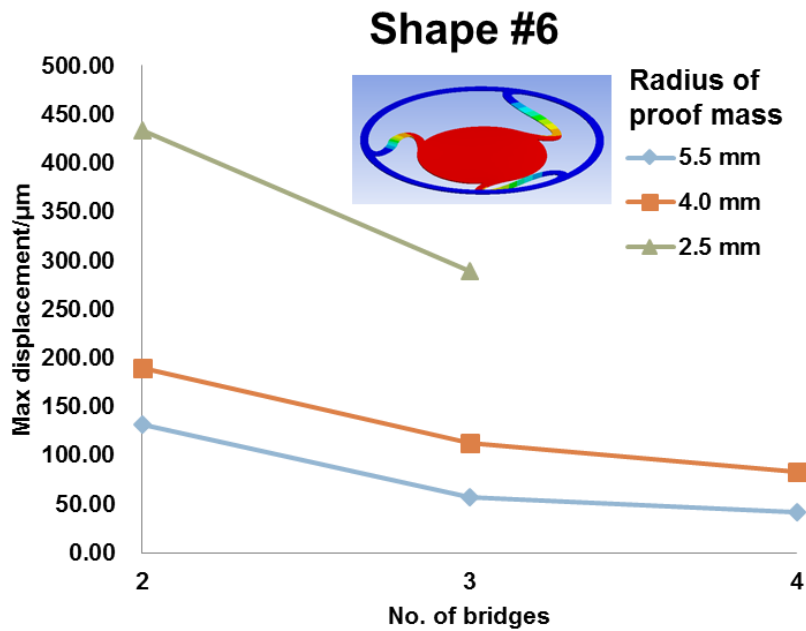
(c) Zigzag line with a corner angle of 90°



(d) Round shape



(e) Eclipse with a ratio of major to minor of 2.8









(f) Eclipse with a ratio of major to minor of 4.8

Figure 2-4 (a-f) Displacement simulation with 20 Pa loading depending on different radius of proof mass, different shapes and numbers of bridge in top membrane

Simulation results in Figure 2.4 demonstrate that smaller number of bridges results in higher displacement of proof mass at the response to applied pressure, which is consistent with theoretical analysis. And, Table 2.1 gives the summarized simulations results for those samples with only 2 bridges.

Table 2-1 Summarized results for samples with only 2 bridges

Samples	radius of proof mass (mm)	Shape of bridges	Max Displacement of proof mass (μm)
#1	5.5		107.35
#2	4.0		63.43
#3	2.5		43.19
#4	5.5		94.32
#5	4.0		64.81
#6	2.5		46.97
#7	5.5		88.84
#8	4.0		82.64
#9	2.5		53.99
#10	5.5		88.13
#11	4.0		76.07
#12	2.5		53.51
#13	5.5		103.06
#14	4.0		141.84
#15	2.5		153.06
#16	5.5		131.64
#17	4.0		189.02
#18	2.5		433.41

As indicated in equation 2.8, both radius of proof mass and effective length (represented by bridge shape) play an important role in the device's mechanical

sensitivity. In Table 2.1, for first 4 bridge shapes, while the radius of proof mass decreases, the max displacement of proof mass decreases. However, for last 2 eclipse bridge shapes, a decreasing radius of proof mass results in a larger displacement. It can be explained that a much larger increase of effective length of bridge in last 6 samples with eclipse bridge shapes increased displacement when the radius of proof mass decreases.

Additionally, we fix the radius of proof mass to 2.5 mm, and summarize the results for samples with varying shape and number of bridges in figure 2.5.

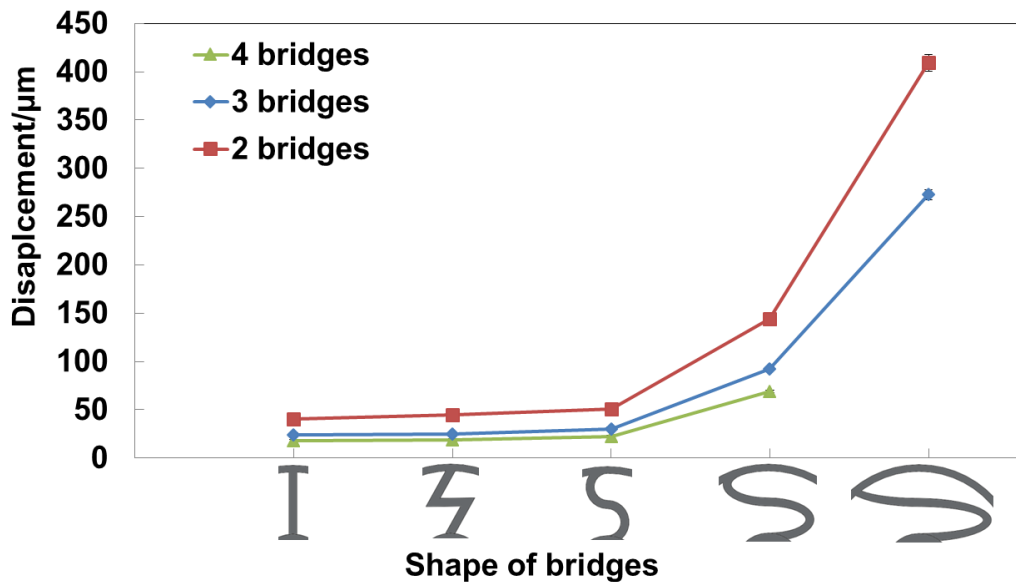
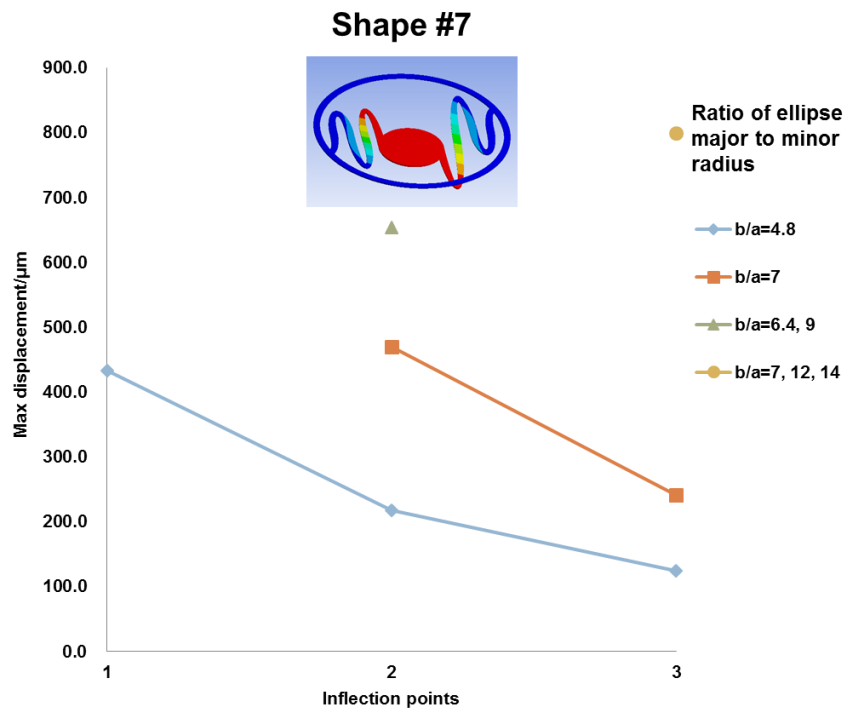


Figure 2-5 Summarized displacement simulation results for samples with different shapes and numbers of bridge. [93]

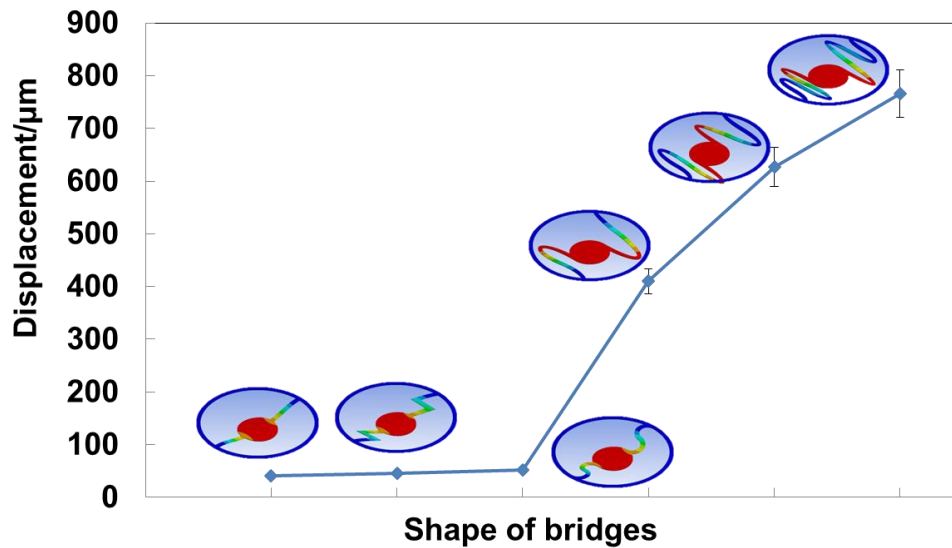
As shown in Figure 2.5, larger length of bridges by changing the patterns of bridges lead to much higher displacement of proof mass. Plus, by varying the radius of proof mass and the shape of bridge together, the highest $\Delta d'$ of is obtained by the sample with a proof mass's radius of 2.5 mm and two longest ellipse shaped bridges.

Next, much longer bridges are introduced to the top membrane design for higher sensitivity. The length of bridges is increased by changing the shape of bridges to ellipse shape with more inflections so as to get longer effective length of bridges. Plus, the

radius of proof mass and the number of bridges are fixed to 2.5 mm and 2 respectively in all samples under test this time. The chosen radius curvature of ellipse demonstrates the longest possible length and smallest radius curvature to have more inflections inside of limited space between ring and proof mass. More simulations with added new shapes of bridges are run in ANSYS under same test conditions. Simulation results are shown in figure 2.4.



(a) Eclipse with different inflections



(b) Summary of samples with varying shape of bridges

Figure 2-6 *Displacement simulation of circular proof mass with 20 Pa pressure load with different shapes of bridge in top membrane*

Similarly, top membranes with longer bridges show much larger deformation, which means much higher sensitivity of the whole devices. The membrane with 2 bridges whose shape is eclipse with 3 inflections exhibits the largest displacement.

In addition, images illustrating different patterns in Figure 2.4(b) show the distribution of displacement in top membranes by gradient colors. Samples with eclipse bridges all show uniform distribution of displacement of center proof mass. Moreover, the sample with 3 inflections presents the most uniform distribution of displacement of the proof mass, which means the least change of overlapped area between movable plate electrode and bottom electrode.

In summary, we design a greatly simple membrane-type flexible accelerometer with a basic configuration of two parallel plate electrodes based on capacitive sensing mechanism. First, analytical equations on capacitive change with respect to accelerations are derived from the structure design of the device. From those equations, some parameters such as length and width of suspension beams in the mechanical structure are highly related to the sensitivity. Next, the design of the membrane is

selected by changing the radius of proof mass, the number and shapes of suspension bridges in top membrane and further simulations in ANSYS. The simulation results show that the sensitivity to accelerations can be enhanced by selecting suspension beams' shapes with longer effective length and decreasing the number of bridges. Consequently, the accelerometer with two extended double ellipse shape suspension beams exhibits the best performance in sensitivity.

Chapter 3.

Fabrication and Characterization of Membrane-based Paper Accelerometers

3.1. Introduction

Silicon-based materials (e.g. single crystal silicon and silicon dioxide) are by far the primary materials used for constructing accelerometers [54, 92]. For flexible accelerometers, we need to find a new alternative to serve as flexible substrates. Paper, the cheapest and most widely used flexible substrate in daily life, have many unique advantages beyond other flexible materials. The speed of the R2R manufacturing process of paper sometimes exceeds 100 km/h [94]. In addition to this, paper is also extremely light-weight and environmentally friendly, since it is recyclable and made of renewable raw materials. Since we are aiming at disposable biomedical sensors, some problems with paper substrate like crinkling or being not that compliant could be negligible. And in recent researches some paper-based MEMS devices have shown similar performance as silicon-based devices [90, 91]. Owing to its brilliant features, paper has been chosen as the basis of this exploratory flexible device.

Conventionally, accelerometers are fabricated using micro machining techniques based on rigid substrates like silicon or silicon nitride. However, such micro fabrication techniques are time-consuming, and require expensive clean room processes by using mask aligners, plasma etchers, and thin-film deposition equipment, and considerable infrastructure. Plus, high processing temperature and several chemical developers in those conventional micro fabrication techniques are not suitable for paper substrates which construct accelerometers in this work [95].

Nano-manufacturing such as nano ink printing technologies (e.g., jet printing,

stamping, spraying, and screen printing), due to their cost-effective and process-effective fabrication, highly meet the requirements for manufacturing of low-cost flexible paper-based accelerometers [96, 97]. Among novel printing techniques, spray coating offers a simple and inexpensive deposition method at room temperature without complex equipment. In addition, in terms of conductivity, silver nanoparticles exhibits the best performance in preparation of thin film metal electrodes among conductive nano-materials. For those reasons, we fabricated metal electrodes for a flexible accelerometer by spraying of silver nanoparticle ink onto the paper substrate.

This chapter introduces manufacturing processes of paper membrane-based accelerometers and further electro-mechanical characterization on sensors to obtain their working frequency range and vibrational sensitivity.

3.2. Fabrication of accelerometers

In previous chapter, the structure design with long ellipse-shaped bridges and round-shaped proof mass shows the best performance in sensitivity to vertical accelerations based on simulation results in ANSYS. Hence, this design is selected for the fabrication of top membrane in the devices. Also, a prototype of sample #18 is prepared for comparison of performance. Plus, four square shape ends are added to top and bottom membranes for electronic interconnection.

Fabrication of accelerometers is divided into three basic steps: patterning of three membranes, preparation of thin-film silver electrodes on top and bottom membranes, and sensor assembly. The process flow of fabrication is depicted in Figure 3.1.

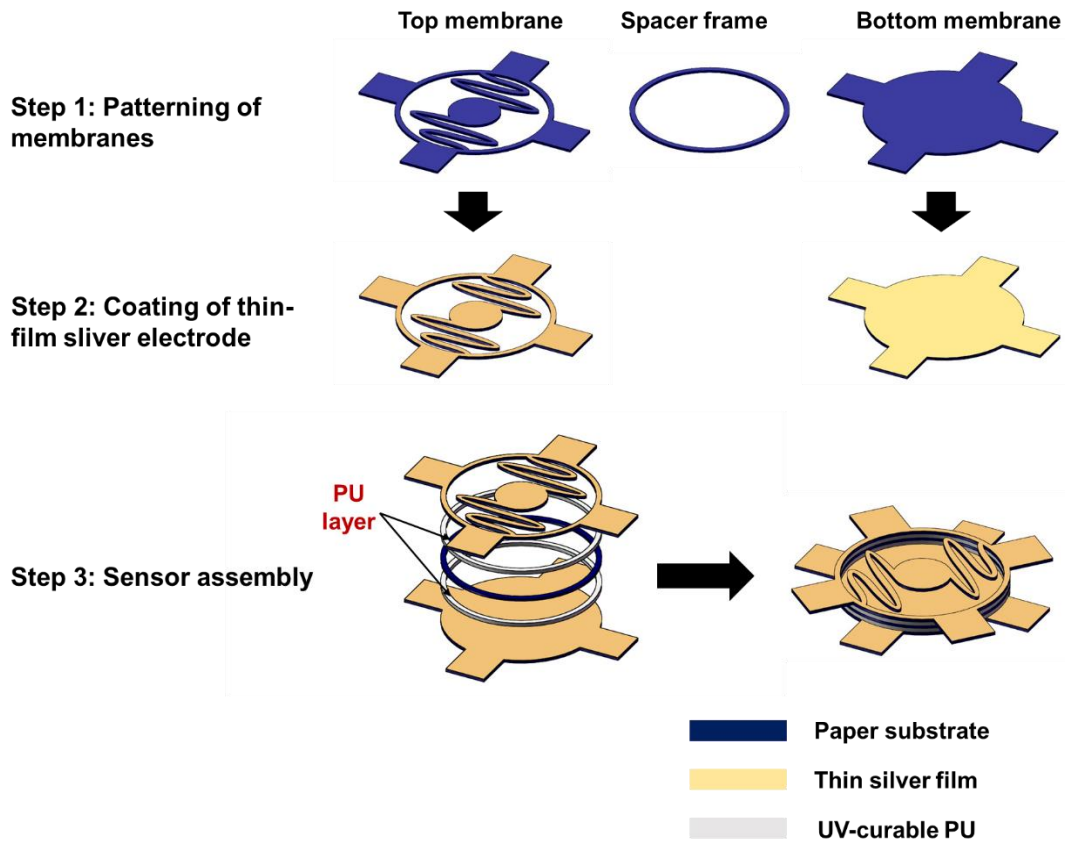


Figure 3-1 Fabrication process flow of accelerometers

3.2.1. Patterning of membranes

Fabrication of accelerometer begins by patterning ring-shape spacer frame, the top and bottom membranes on cellulose paper substrates using by laser cutter (Universal Laser Systems VLS3.60). Cellulose fiber paper substrates are kindly provided from FPInnovations.

First, 2D designs of three membranes are drafted in CorelDraw based on optimized dimensions from previous chapter. Power (68%) and speed (20%) settings in laser cutter are optimized for paper substrates. Then, patterns on membranes are well defined by laser cutting. Figure 3.2 shows images of laser-cut paper membrane examples.

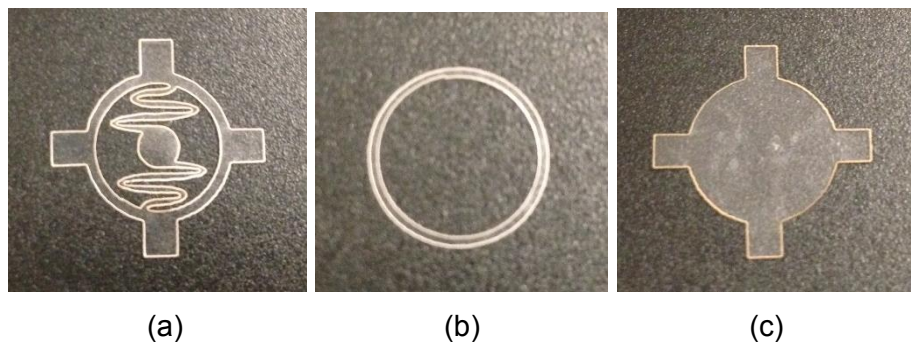


Figure 3-2 *Images of laser-cut paper membranes: (a) top membrane, (b) spacer frame, (c) bottom membrane.*

3.2.2. Preparation of thin-film silver electrodes

Second, a dispersion of silver nanoparticles (AgNPs) in toluene (5 wt. %) is prepared as silver nano ink. AgNPs are synthesized as previously reported [97]. Then, silver nano ink is directly sprayed onto top and bottom pre-patterned membranes as shown in Figure 3.3. The solvent for AgNPs evaporates soon after sprayed. A thin layer of silver nanoparticles is homogeneously deposited on both membranes.

The printed features comprising of silver nanoparticles are annealed in an oven at 160 °C for 10 min, resulting in the formation of thin film silver electrodes on the surface of both membranes.

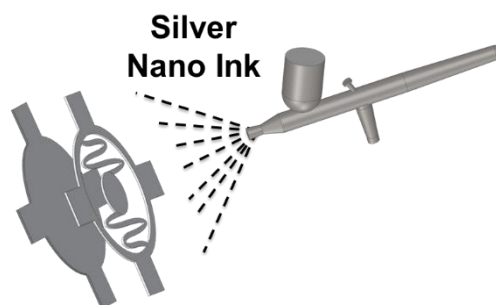


Figure 3-3 *Schematic illustration of spraying of silver nano ink on top and bottom membranes. [93]*

The conductivity of the resulting silver films on two membranes is measured by 4-probe method. Finally, the annealed electrode from this AgNPs ink shows a conductivity of about 1.5×10^4 S/cm, which is notably close to the conductivity of bulk

silver (6.3×10^5 S/cm). As a result, two membrane electrodes with superb conductivity are successfully generated on paper substrates by spray coating of silver nano ink.

3.2.3. Sensor assembly

Next, two membrane electrodes on cellulose paper and spacer frame are aligned well and bonded together with UV-curable polyurethane resin as illustrated in step 3 in Figure 3.1. With separation by one spacer frame and two PU layers, the top membrane is suspended above a 1mm gap from the bottom membrane.

Finally, the assembled accelerometer is completed after exposure of UV light on polyurethane resin. The whole device is exposed to UV light (365 nm wavelength) offered by high-intensity UV lamp (Blak-Ray™ B-100AP) for 1 min such that fully cured PU layers bond three membranes together to create final assembly. UV-curable polyurethane (PC7010) was purchased from Polysciences, Inc.

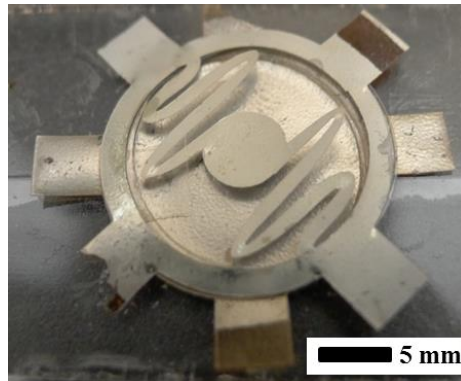
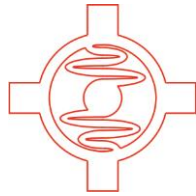
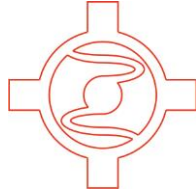


Figure 3-4 Image of assembled device. [93]

In total, three devices have been assembled using the aforementioned fabrication process. For device #1 & #2, considering that the size of proposed accelerometers is a bit bulky for unobtrusive sensing, two devices with different dimensions are fabricated for further investigation. For device #1, the radius of ring shape membrane is 7 mm and the radius of proof mass is 2.5mm. Device #2 with same configuration but half size in total is fabricated with same process flow. Image of a representative assembled device #1 is shown in Figure 3.4. For device #3, it's fabricated based on the design of sample #18. Dimensions of three devices are shown in table 3.1.

Table 3-1 Dimensions of three devices

Devices	Radius of anchor ring	Radius of proof mass	Shape of bridge
#1	7 mm	2.5 mm	
#2	5 mm	1.8 mm	
#3	7 mm	2.5 mm	

3.3. Characterization of accelerometers

The fabrication of devices is followed by characterization on different electro-mechanical parameters in order to test their performance in different aspects.

First, the capacitance value at the initial position of the sensor is measured by LCR meter (Agilent E4980A). The initial capacitance of device #1 and device #3 is about 5.92 pF and 5.10 pF; and the initial capacitance of device #2 is about 3.14 pF. Next, accelerometers are tested under vertical accelerations to obtain their working frequency range and measure sensitivity to vibrations.

3.3.1. Optimal working frequency range

For further applications in different fields like biomedical sensing, a proper working frequency range for accelerometers is an essential consideration. Therefore, vibration testing is conducted on accelerometers toward obtaining a working frequency range. The resonant frequency of two accelerometers is measured so as to decide their optimal working frequency range.

3.3.1.1 Analytical calculations

Since all the dimensions of accelerometers are either measurable or already known, the absolute value of resonant frequency of sensors in the sensing direction can be estimated based on mechanical analysis.

As a second-order mass-spring-damper system, the resonant frequency of the accelerometer can be expressed as [52]

$$f = \frac{1}{2\pi} \sqrt{\frac{k_0}{m}} = \frac{1}{2\pi} \sqrt{\frac{nk}{\rho\pi r^2 t}} \quad , \quad (3.1)$$

where k_0 is the spring constant of entire system and m is the effective proof mass of accelerometer.

From equation (2.3), the values of spring constant of suspension beams in device #1, #2 and #3 are given by

$$k_1 = \frac{3EI}{L_1^3} \quad , \quad (3.2)$$

$$k_2 = \frac{3EI}{L_2^3} \quad , \quad (3.3)$$

$$k_3 = \frac{3EI}{L_3^3} \quad (3.4)$$

where k_1 and L_1 are the spring constant and effective length of bridges in device #1; k_2 and L_2 are the spring constant and effective length of bridges in device #2; k_3 and L_3 are the spring constant and effective length of bridges in device #3. And t , and E are the same in three devices.

Substituting k_1 , k_2 and k_3 into equation (3.1), we have resonant frequency

$$f_1 = \frac{1}{2\pi} \sqrt{\frac{nk_1}{\rho\pi r_1^2 t}} = \frac{1}{2\pi} \sqrt{\frac{3nEI}{\rho\pi r_1^2 t L_1^3}} \quad , \quad (3.5)$$

$$f_2 = \frac{1}{2\pi} \sqrt{\frac{nk_2}{\rho\pi r_2^2 t}} = \frac{1}{2\pi} \sqrt{\frac{3nEI}{\rho\pi r_2^2 t L_2^3}}, \quad (3.6)$$

$$f_3 = \frac{1}{2\pi} \sqrt{\frac{nk_1}{\rho\pi r_3^2 t}} = \frac{1}{2\pi} \sqrt{\frac{3nEI}{\rho\pi r_3^2 t L_3^3}} \quad (3.7)$$

where f_1 , f_2 and f_3 are the resonant frequencies of device #1, #2 and #3 respectively; r_1 , r_2 and r_3 are the radius of proof mass in device #1, #2 and #3 respectively.

As the effective length L_1 of bridge in device #1 is longer than that in device #2, k of bridge in device #2 is smaller than that in device #1. Plus, the radius of proof mass r_1 in device #1 is larger results in lower resonant frequency based on equation (3.4) and (3.5). In consequence, the resonant frequency f_1 of device #1 is lower than f_2 . Similarly, as the effective length L_1 of bridge in device #1 is longer than that in device #3, the resonant frequency f_1 of device #1 is lower than f_3 .

3.3.1.2 Experiments and results

Next, experiments are conducted to inspect and verify the analyzed values of resonant frequency. Vibration tests are performed on three sets of optimally fabricated devices. A shaker (Brüel & Kjær LDS V408) is used to provide vibration testing of accelerometers with accelerations over a wide frequency range. A schematic description of the experimental setup for characterization of accelerometers is illustrated in figure 3.5.

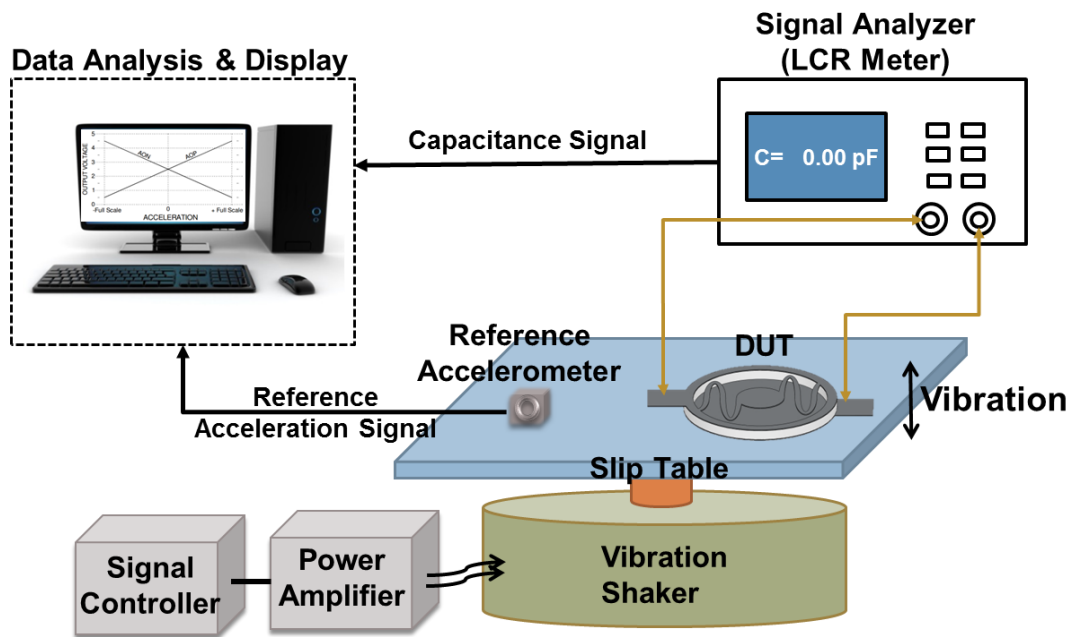


Figure 3-5 Schematic diagram of the experimental set-up for vibration testing.

For testing purposes, accelerometers are rigidly mounted to onto a plexiglass fixture with two mounting screws attached to the shaker table. The amplitude and frequency of vibration is amplified by power amplifier and controlled by signal controllers. And the acceleration of the table is detected by a commercial reference accelerometer integrated in the shaker.

One end of either membrane electrode is connected to the LCR meter via aluminum film for capacitance measurement. Figure 3.6 shows photographs of the installation of accelerometers with interconnections on shaker table.

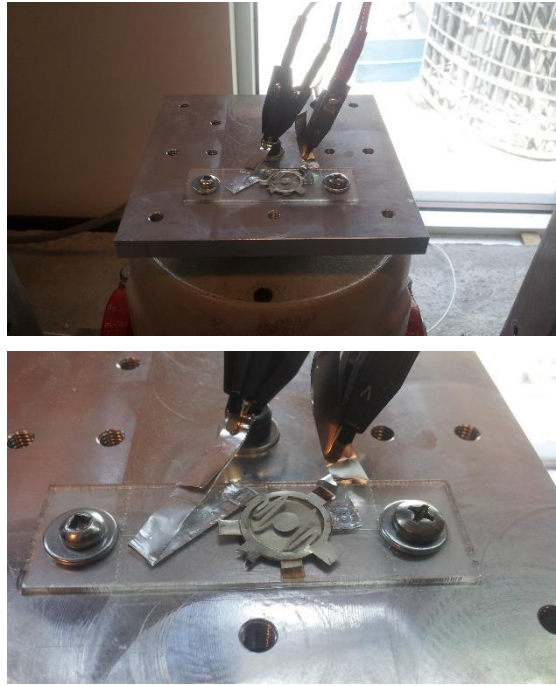


Figure 3-6 *Photographs of accelerometers connected to LCR meter on shaker table.*

The shaker vibrates the accelerometer at chosen amplitude over a specified frequency range (10-180 Hz). In response to the applied external z-axis acceleration, the proof mass vibrates along the direction normal to the bottom electrode. In the meantime, the capacitance change of two devices is measured by LCR meter.

First, the vibration amplitude of the shaker table is fixed, and frequency is sweeping from 10 Hz to 180 Hz. Thus, the frequency under which the accelerometer reaches the highest ΔC supposes to be the resonant frequency. The measured capacitance changes of three different devices as a function of different frequencies are shown in Figure 3.7 and Figure 3.8.

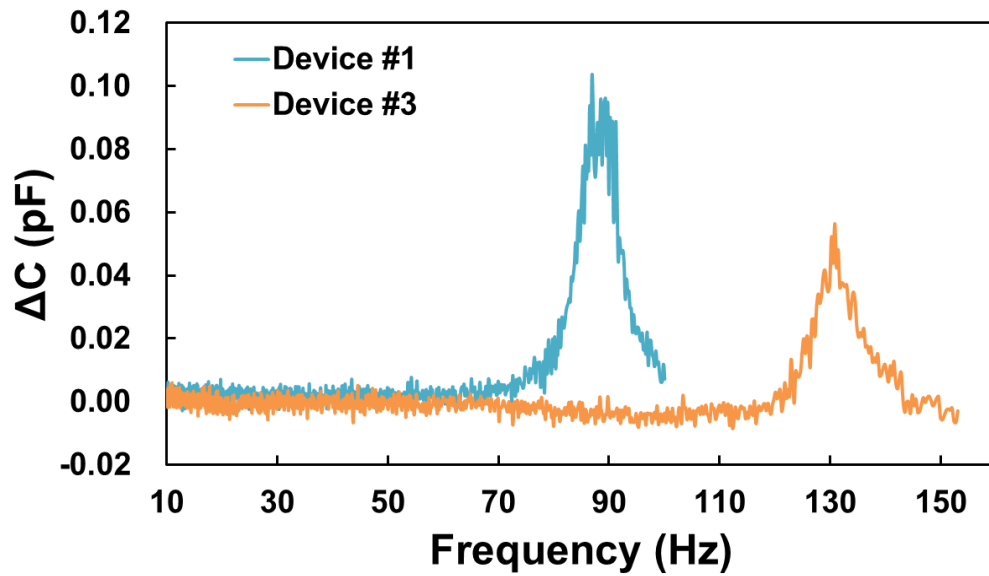


Figure 3-7 Capacitance changes of two accelerometers with different bridges in response to sweeping frequency from 10 Hz to 180 Hz

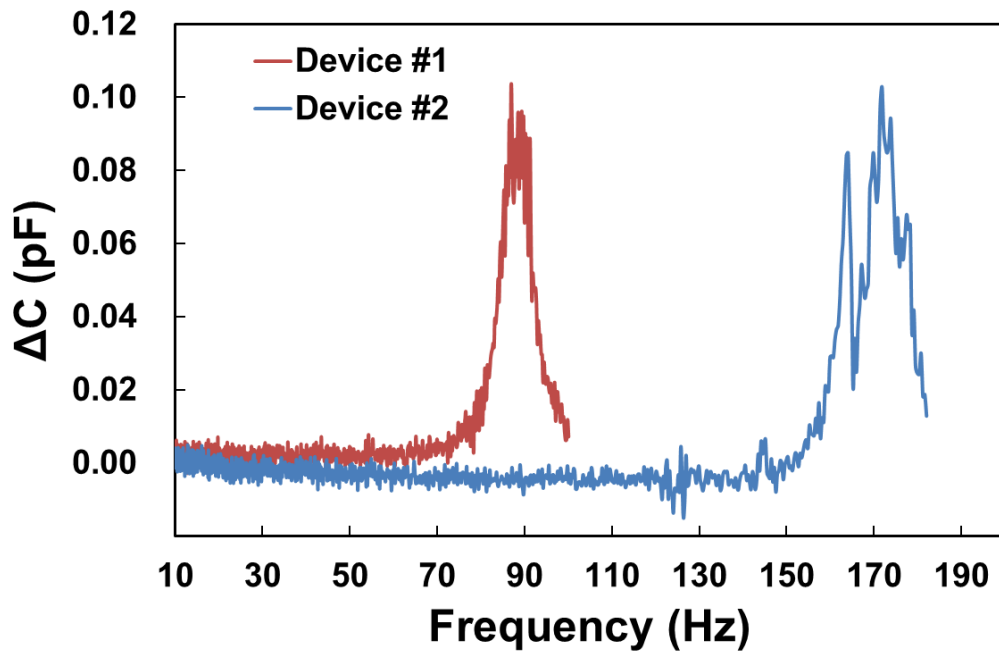


Figure 3-8 Capacitance changes of two accelerometers with different sizes in response to sweeping frequency from 10 Hz to 180 Hz. [93]

From the measured ΔC response in Figure 3.7, the resonant frequencies of device #1 and device #3 are captured to be approximately 90 Hz and 130 Hz, respectively. And from the ΔC response in Figure 3.8, the resonant frequency of device

#2 is captured to be 171Hz. Those experimental results match the previous theoretical analysis that f_1 is lower than both f_2 and f_3 . The measured values of resonant frequencies of three devices are shown in Table 3.2.

Table 3-2 Mechanical parameters for accelerometers in two sizes

Devices	Resonant frequency	Optimal working frequency range	Vibrational sensitivity
#1	90 Hz	< 70 Hz	0.021 pF/g
#2	171 Hz	< 150 Hz	0.011 pF/g
#3	130 Hz	< 120 Hz	0.012 pF/g

In addition, since working frequency of accelerometers should be well below the resonant frequency, an optimal working frequency range can be extracted from the mechanical response of accelerometers in Figure 3.7 and Figure 3.8. The extracted values are shown in Table 3.2. For all those three devices, the working frequency range fits the frequency range used in biomedical applications.

3.3.2. Vibrational sensitivity

From equation (2.6), a linear relation between the applied acceleration and the displacement of proof mass exists such that Δd increases when a increases. Hence, a larger deflection of top electrode leads to a larger capacitance change. Also, we can acquire an estimation of sensors' vibrational sensitivity by means of measuring capacitance change response to increasing amplitude of acceleration.

Additionally, from equation (2.6), since r and L_{eff} in device #1 are larger than those in device #2, at each acceleration point device #1 exhibits a larger Δd , hence, a larger ΔC . Also, since effective length of bridge L_1 in device #1 is larger than that in device #3, device #1 exhibits a larger ΔC at each acceleration point.

Next, we fix the frequency at the resonant frequency and change the vibration amplitude of the shaker so as to get ΔC of the devices at response to different accelerations under same frequency. Resonant frequencies are chosen as the vibrational frequency such that proof mass oscillates at the highest amplitude resulting in a high enough non-noise ΔC signal of the accelerometer.

For three devices, the shaker is excited using sinusoidal signal at their resonant frequencies with the same experimental setup. The shaker vibration is conducted at 10 different amplification points generating different maximum accelerations in a range of 1-10 g. 10 g is the maximum range of the shaker. The relation between the measured capacitance changes and corresponding excited accelerations in devices is presented in Figure 3.9.

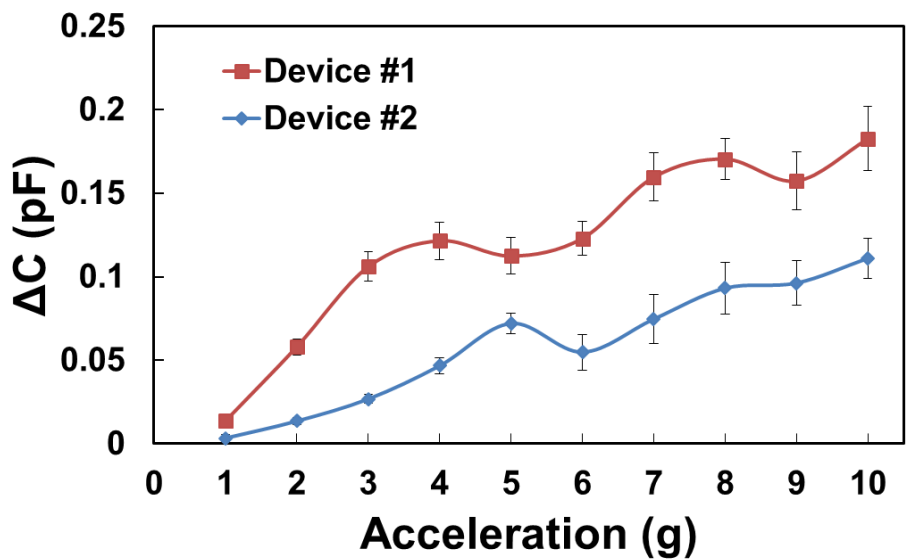
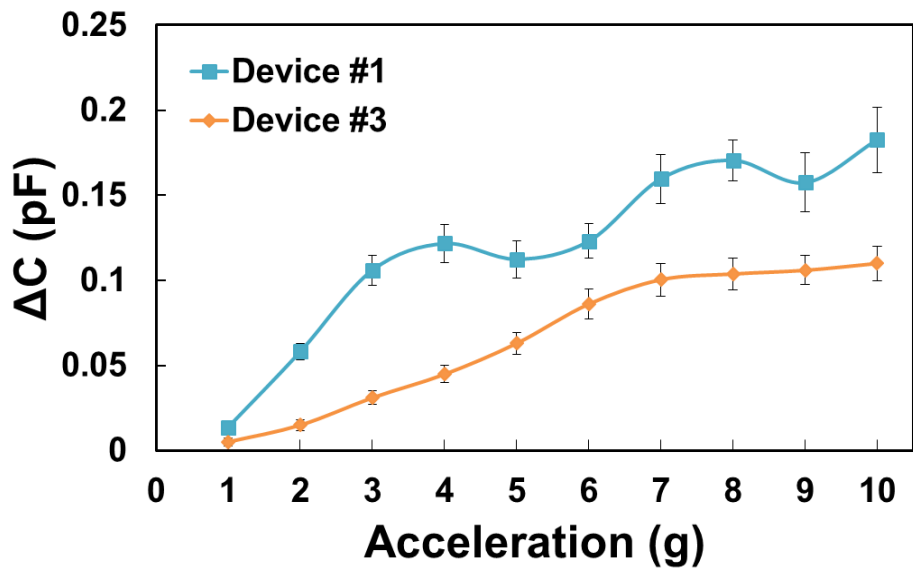


Figure 3-9 Capacitance response of three accelerometers over a range of 1–10 g acceleration. [93]

As we expect, the capacitance change ΔC increases when the accelerometer is excited with larger acceleration in both cases. And, the capacitance change of device #1 is always larger than that of device #2 and device #3. Values measured beyond 5 g show slight fluctuation of ΔC at certain acceleration points. This localized slow increase might come from interference with generated noisy sound of shaker starting from around 5 g.

As shown in Figure 3.9, the relation between capacitance change and amplitude of acceleration is significantly close to be linear. Then, linear regression line in the form of $y=ax$ is set up for both curves in Figure 3.9. As a result, the slope of regression line is considered as the sensitivity to vertical accelerations.

The capacitive sensitivity of device #1 is about 0.021 pF/g, and that of device #2 is about 0.011 pF/g over an acceleration range of 1–10 g in the z-axis. When we utilize this flexible accelerometer technology as a motion or pulse detector of human in biomedical applications, the devices can be good candidates with higher sensitivity and lower resonant frequency close to human's moving frequency (less than 60 Hz) and pulsing rate (less than 2 Hz).

In conclusion, highly sensitive membrane-type flexible paper accelerometers are fabricated by facile spraying techniques with silver nano ink. Resonant frequencies of the fabricated devices are found to be in the range of 90-170 Hz. Also, accelerometers show a measured sensitivity of 0.01–0.02 pF/g under the accelerations ranging from 1 g to 10 g at their resonant frequencies.

Chapter 4.

Integrated Accelerometer System for Biomedical Sensing Applications

4.1. Introduction

Wearable health monitoring systems have gathered considerable attention from both academia and industry in recent years mainly because of the increasing healthcare costs and the aging global population [98]. A wearable system can drastically reduce the expenses on personal health care by providing pervasive, 24-hrs monitoring of physical activities and significant physiological parameters, like heart rate, blood pressure, body temperature, respiration rate, etc. Monitoring of one's long-term physical activities, such as body movement, can provide paramount information indicative of mobility level, latent chronic diseases and aging process [80]. Moreover, heart rate and heart interval profile can offer essential data for early diagnosis of cardiovascular diseases [84].

Accelerometers have found widespread use in biomedical applications, especially in health monitoring applications [75, 77, 99]. First of all, accelerometers have been widely accepted as useful and practical motion detectors for the use of human movement measurement. Within the last several years, accelerometers are commercialized in the market to help determine the speed and distance for the runners wearing units containing sensors and also calculate gait parameters, such as stance and swing phase.

Second, recent advances in MEMS technology have shown that accelerometers can be also used as heart rate [100] and heart sound monitoring systems [101]. From those development in this field, accelerometers have demonstrated their great potential in measuring or monitoring a variety of clinical characteristics of people.

Taken into account the flexibility and extremely lightweight of constructing materials for our proposed accelerometer, paper accelerometer is a superior candidate as wearable sensors in health monitoring systems. And, device #2 in chapter 2 is chosen as the sensor in following studies because of its relatively smaller size.

In this chapter, we demonstrate a highly sensitive, and directly attachable accelerometer system suitable for extracorporeal sensing, such as motion detection, and heart rate. A readout circuit is integrated with the sensor system to convert capacitance changes to amplified voltage signals. The high sensitivity enables this sensor system to precisely detect various human pulses and body movement.

4.2. Integration with readout circuit

As we discussed, the air gap between the movable proof mass and the fixed bottom electrode changes when an external acceleration (normal to the proof mass) is applied to the entire device. A change in the air gap causes a change in capacitance between the electrodes. To produce an electrical response, this change in capacitance is converted to an electrical voltage using a readout circuit integrated with mechanical sensors.

4.2.1. Circuit design

Since the capacitance of the accelerometer is very small (1-10 pF), a readout circuit is designed and integrated to be able to amplify and read the voltage change converted from the capacitance change. Figure 4.1(a) shows the schematic of the circuit design where a variable capacitor represents the accelerometer. The circuit is consisting of basic electronic components including resistors, capacitors, diodes and operational amplifiers (op-amps).

Based on the design, the circuit is built on a compact breadboard, and is connected to the printed accelerometer by thin magnet wires (Gauge 36) as shown in Figure 4.1(b). The interconnection between ends on membrane electrodes and thin wires is achieved by silver paste.

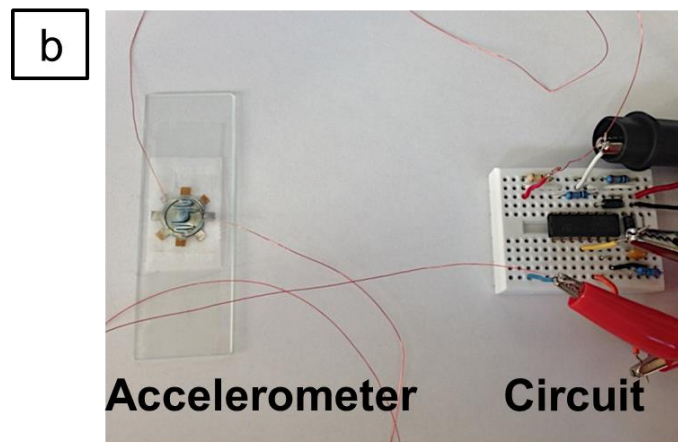
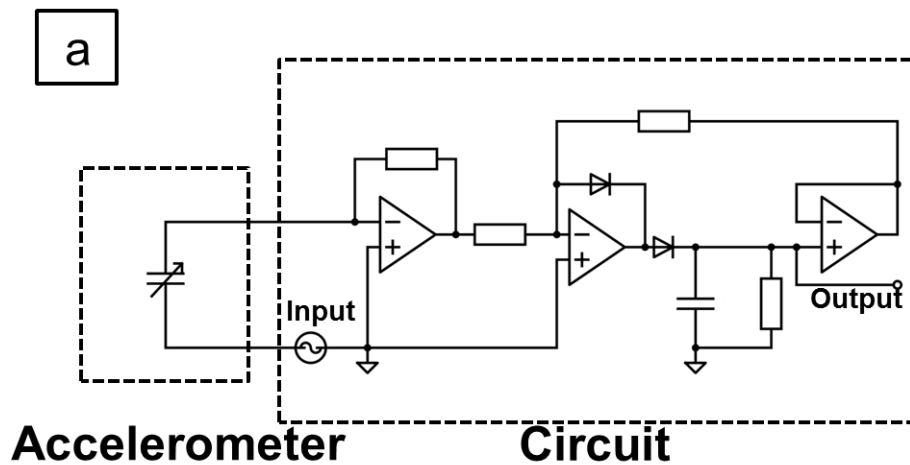


Figure 4-1 (a) Schematic diagrams of accelerometer (left) and readout circuit design (right); (b) Fundamental experimental setup that printed accelerometer is connected to readout circuit on breadboard via magnet wires.

First, a sinusoidal voltage signal is generated by a function generator (GWINSTEK GFG-3015). As the capacitance of the sensor changes, the current through the capacitor changes. Then, the current change is converted to a voltage signal and amplified through a trans-impedance amplifier that composes of two resistors and one op-amp.

To output a DC voltage signal, the current-to-voltage converter is followed by a precision peak detector that detects the positive peak of the input. Finally, the amplified DC voltage change is acquired by a Keithley 2400 source meter. Average filter function

in Keithley 2400 is used to filter some noise from the circuit. After filtration, the noise level is smaller than 0.0005V.

In further studies, the designed circuit can be built on a much thinner and lighter board instead of this bulky breadboard. Also, a wireless module can be integrated with the accelerometer system to achieve wireless communication between the sensor and signal processing platforms like smart phones and tablets.

4.2.2. System validation

Validation of this integrated accelerometer system is accomplished by manually changing the gap between two membrane electrodes and inspection of voltage output from the readout circuit. The approach is similar to the simulation performed on modeled sensor architecture in ANSYS from Chapter 2.

The experiment is conducted by periodical pressing on the proof mass with different pressure loads using a digital force gauge (Dillon Model GS) with hand wheel test stand. While the gap between proof mass and bottom electrode is changing, the voltage change derived from capacitance change is real-time recorded.

Due to the extremely lightweight of paper membrane electrode, the damping force from top membrane is very small. Hence, the pressure load needed to deflect the proof mass is almost zero shown on the display of force gauge. Voltage output characteristics at different types of pressure loads are given in Figure 4.2. The forces of both pressing with 0.5 mm in depth and pressing with 0.3 mm in depth are smaller than the minimum scale (0.005N) of force gauge.

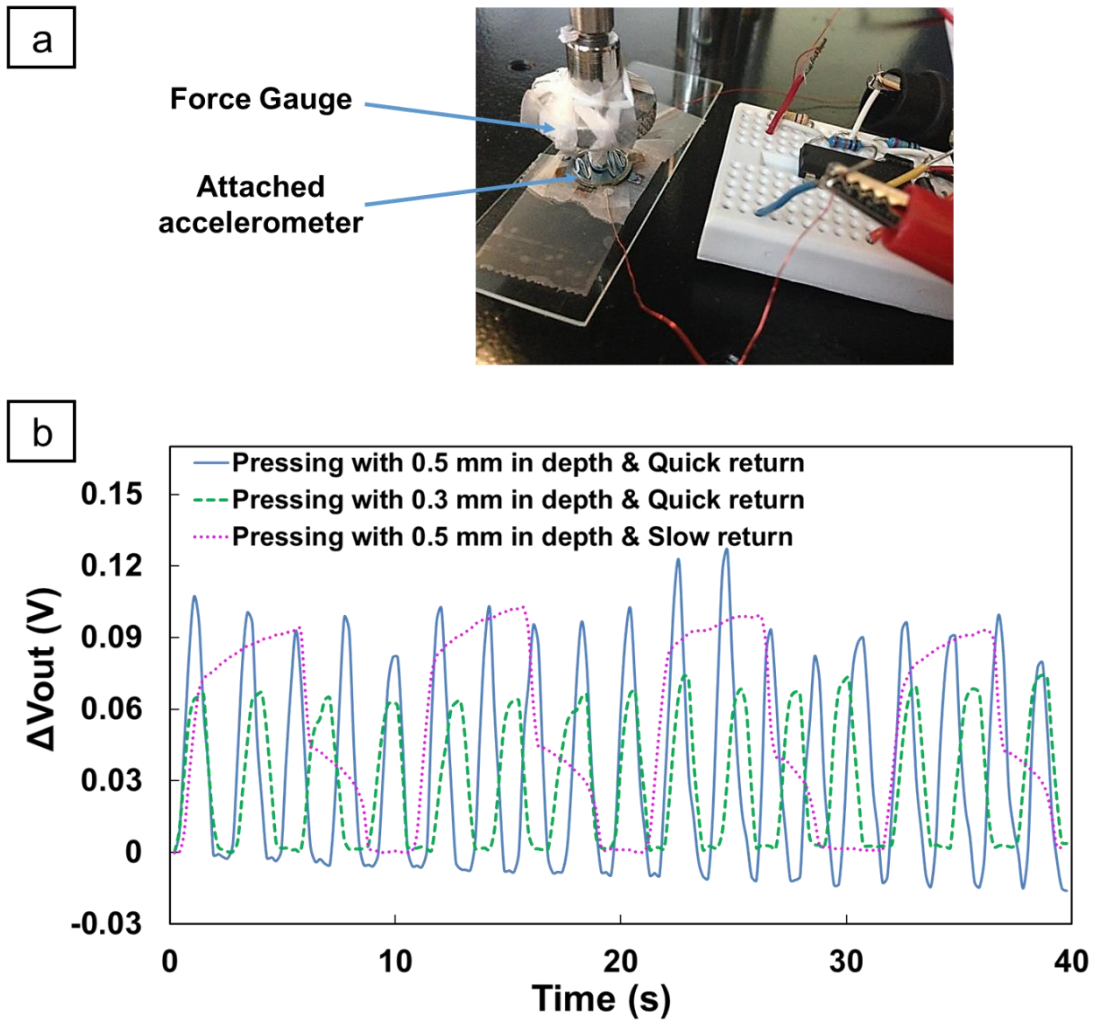


Figure 4-2 (a) Experimental setup of pressing test. (b) Sensor response during repeated pressing and releasing. Green: slight press and quick release; Magenta: press the proof mass to the same level, maintain for 5s and then slow release; Blue: press the proof mass to a relatively high level and quick release. Inset is experimental setup of pressing test.

In several pressing cycles, the capacitive sensor shows an instantaneous response to the change of the applied pressure. When the proof mass deflects toward the bottom electrode, the capacitance decreases resulting in increasing the voltage output correspondingly. Also, when the deflection of proof mass decreases, the voltage output is reduced as expected.

From those pressing test results, we notice that the entire accelerometer system is working properly to obtain a voltage output signal proportional to the variable gap between the proof mass and bottom electrode.

4.3. Comparison the paper-based sensor with a commercial silicon-based MEMS sensor

In previous chapter, at the resonant frequency of 171 Hz, the sensitivity of device #2 is approximately 0.011 pF/g. Integrated with readout circuit, below 40 Hz, the accelerometer exhibits a response with a sensitivity in the range of 2-3 mV/g.

Commercially available silicon-based accelerometers provide a sensitivity of a few hundred mV/g using integrated electronics with high gain amplifiers. The sensitivity of the accelerometer could be improved by using capacitance-to-voltage readout chip with a high amplification factor. This accelerometer is usable in the frequency range of up to 150 Hz.

Table 4.1 lists specifications of a commercial single-axis MEMS silicon accelerometer and our paper-based accelerometer. Both sensors are based on capacitive sensing. The commercial sensor is fabricated in silicon using standard micro machining technology. From table 4.1, our paper-based sensor has a lower acceleration measurement range and sensitivity than the commercial counterpart, but it has lower cost and requires much simpler fabrication process. In consideration of fabrication and cost, our proposed paper-based paper accelerometer may provide a less expensive and process-effective solution for typical acceleration sensing applications than a silicon-based MEMS sensor. Additionally, the flexible nature of paper may promise the paper-based sensor to be used in wearable sensing applications.

Table 4-1 Comparison of specifications of a commercial single-axis silicon-based MEMS accelerometer (Analog Devices ADXL001) and our paper-based printed accelerometer

Specifications	Commercial silicon MEMS accelerometer (Analog Devices ADXL001)	Paper-based printed accelerometer
Sensing principle	Capacitive	Capacitive
Material	Silicon	Paper
Resonant frequency	22 kHz	171 Hz
Acceleration range	$\pm 70g$	$\pm 10g$
Sensitivity	16 mV/g	~ 2 mV/g
Fabrication process	>1 day in clean room	<3 hours in laboratory

4.4. Potential biomedical applications

4.4.1. Motion detection

Since the accelerometer system is working properly, it can be utilized as a motion sensing system that is the most common application for accelerometers. And, this application can also test the sensitivity of accelerometers to tiny movement as a preliminary assessment for further pulse measurement. The working principle is illustrated in Figure 4.3.

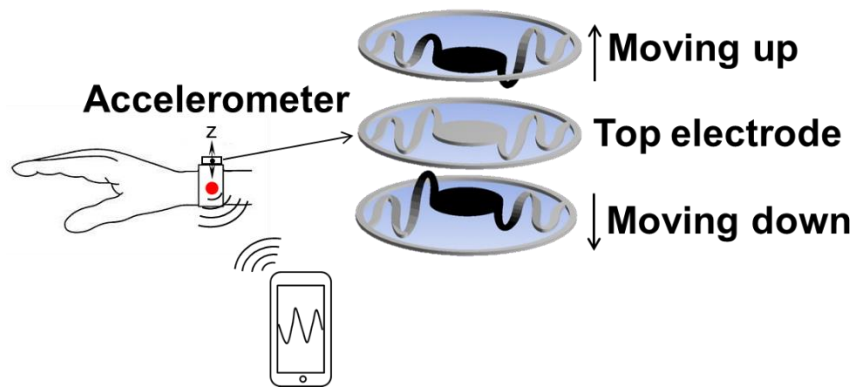


Figure 4-3 *Schematics of the working principle of motion detection by the accelerometer (top electrode deforms when moving up or down) and the concept of wireless monitoring.*

In Figure 4.3, the sensor system is mounted onto the human forearm by several rubber bands in order to detect motion of the forearm. When the forearm goes upwards an acceleration in the direction normal to the forearm is given to the sensor system such that the gap between two electrodes decreases due to inertial. Therefore, the capacitance decreases and results in an increasing voltage output from the readout circuit. Then, the gap goes back to the initial position when the forearm goes downwards, which leads to a decreasing voltage signal. Also, when the forearm comes to the up position, the voltage reaches the peak level and vice versa. Therefore, the accelerometer system is capable of detecting human motion with different amplitudes and frequencies.

4.4.2. Pulse measurement

Human pulse represents how many times a minute that our arteries expand because of the increase in blood pressure originated by our heartbeat. The pulse can be found at any place that allows an artery to be compressed against a bone, such as at the neck (carotid artery), the wrist (radial artery), on the inside of the elbow (brachial artery), behind the knee (popliteal artery), etc.

Pulse is equivalent to the rate of heart contractions. According to the report [102], the normal heart rate range for adults is 60-100 beats per minute ($f = 1-1.67$ Hz), which falls in the working frequency range of our propose accelerometers. The instantaneous

detection of minute movement of the fabricated accelerometer system imply that this system is exactly suitable for extracorporeal sensing, for instance in PPG with human pulse detection.

4.4.3. Heart rate and respiratory rate

This technique is mainly relying on the change from the blood vessels due to the pulse in cardiovascular system. In pulse measurement, we can conformally attach our accelerometer similarly like attaching a bandage to different pulsation points on human body such as the neck (carotid artery), the inside of the elbow (brachial artery), and chest near heart.

Also, this sensor can also detect the respiratory rate, one of the four main vital signs, which represents the number of breaths (inhalation-exhalation cycles) a person takes within one minute. Normal respiration rates for a healthy adult at rest range from 18 to 22 breaths per minute [102].

As a result, the integrated accelerometer system has its potential of monitoring heart rate and respiration rate simultaneously on the chest near heart. This bandage-type attachable sensor system may allow continuous detection of bio-signals as long-term, continuous medical diagnostics with no obstruction to the patient.

4.5. Conclusion

In conclusion, we design and integrate a readout circuit with the paper-based printed accelerometer. This integrated accelerometer system is working properly to convert vertical accelerations to DC voltage output signal. A real-time pulse wave may be obtained with the attachment of the sensor to several pulsation points to measure heart rate and respiratory rate of human, and is of use for cardiovascular disease diagnostics. Future work in integration with flexible wireless modules will generate a completely flexible, high-fidelity sensor system for applications in wearable wireless health monitoring.

Chapter 5.

Conclusions and Future Work

5.1. Conclusions

The objective of this work is to construct a flexible printed accelerometer system for biomedical sensing applications. First, we propose a structure design of accelerometers that employ parallel-plate capacitive sensing. With selection of many mechanical parameters of top membrane electrode in accelerometers, they obtain a great performance of sensitivity in simulation approach.

Next, paper-based accelerometers with this configuration are fabricated with novel printing technologies including spray-coating with silver nano ink and laser cutting for patterning. Characterization on fabricated devices is done by a series of projected vibration tests. Such process-effective and light-weight accelerometers with two different sizes demonstrate a capacitive sensitivity of 0.01-0.02 pF/g under the accelerations ranging from 1 g to 10 g at a resonant frequency range of 90-171 Hz.

Furthermore, a well-designed interface circuit is integrated with the printed accelerometers to output a voltage signal proportional to the external vertical acceleration. The entire accelerometer system works properly as we expected under a simple pressing test. Compared to commercial silicon-based MEMS accelerometers, although it maintains a lower sensitivity to single-axis accelerations, our proposed paper-based paper accelerometer may provide a less expensive and process-effective solution for typical acceleration sensing applications. Additionally, the flexibility of paper may promise the paper-based sensor potential wearable sensing applications.

5.2. Future work

In some aspects, the proposed accelerometer system can be improved by a few changes or adding more features.

- Implement some signal processing techniques to the acquisition and analysis of pulse waves. Baseline wander is noticeable in all the pulse waves obtained in Chapter 4, and peak or foot of some pulse periods is not that clear to be distinguished. An algorithm based on shifting window can be adopted to remove the baseline wander. After removing baseline wander, we can use a differential threshold algorithm to detect the significant characteristic points of pulse periods.
- Substitute bread board with a much smaller and lighter printed circuit board on which interface circuit is built.
- Integrate interface circuit with a wireless module for wireless communication with processing platforms.

References

- [1] I.C. Cheng, S. Wagner, Overview of Flexible Electronics Technology, in: W. Wong, A. Salleo (Eds.), Flexible Electronics, vol 11, Springer US, 2009, pp. 1-28.
- [2] Y. Zhou, L. Hu, G. Grüner, Applied Physics Letters 88 (2006) 1-3.
- [3] A. Rida, Y. Li, R. Vyas, M.M. Tentzeris, Antennas and Propagation Magazine, IEEE 51 (2009) 13-23.
- [4] J. Vaillancourt, H. Zhang, P. Vasinajindakaw, H. Xia, X. Lu, X. Han, D.C. Janzen, W.-S. Shih, C.S. Jones, M. Stroder, M.Y. Chen, H. Subbaraman, R.T. Chen, U. Berger, M. Renn, Applied Physics Letters 93 (2008) -.
- [5] J. Zhou, Y. Gu, P. Fei, W. Mai, Y. Gao, R. Yang, G. Bao, Z.L. Wang, Nano Letters 8 (2008) 3035-3040.
- [6] T. Rai, P. Dantes, B. Bahreyni, W.S. Kim, Electron Device Letters, IEEE 34 (2013) 544-546.
- [7] L. Gomez De Arco, Y. Zhang, C.W. Schlenker, K. Ryu, M.E. Thompson, C. Zhou, ACS Nano 4 (2010) 2865-2873.
- [8] A. Nadarajah, R.C. Word, J. Meiss, R. Könenkamp, Nano Letters 8 (2008) 534-537.
- [9] Y. Chen, J. Au, P. Kazlas, A. Ritenour, H. Gates, M. McCreary, Nature 423 (2003) 136.
- [10] D.S. Hecht, L. Hu, G. Irvin, Advanced Materials 23 (2011) 1482-1513.
- [11] P. Lee, J. Lee, H. Lee, J. Yeo, S. Hong, K.H. Nam, D. Lee, S.S. Lee, S.H. Ko, Advanced Materials 24 (2012) 3326-3332.
- [12] S. De, T.M. Higgins, P.E. Lyons, E.M. Doherty, P.N. Nirmalraj, W.J. Blau, J.J. Boland, J.N. Coleman, ACS Nano 3 (2009) 1767-1774.
- [13] K. Suganuma, Conducting Materials for Printed Electronics, Introduction to Printed Electronics, vol 74, Springer New York, 2014, pp. 49-74.
- [14] F. Xu, Y. Zhu, Advanced Materials 24 (2012) 5117-5122.

- [15] Y. Sun, B. Gates, B. Mayers, Y. Xia, *Nano Letters* 2 (2002) 165-168.
- [16] L. Hu, H.S. Kim, J.-Y. Lee, P. Peumans, Y. Cui, *ACS Nano* 4 (2010) 2955-2963.
- [17] L. Hu, H. Wu, Y. Cui, *MRS Bulletin* 36 (2011) 760-765.
- [18] G.Y. Margulis, M.G. Christoforo, D. Lam, Z.M. Beiley, A.R. Bowring, C.D. Bailie, A. Salleo, M.D. McGehee, *Advanced Energy Materials* 3 (2013) 1657-1663.
- [19] K. Jiang, J. Wang, Q. Li, L. Liu, C. Liu, S. Fan, *Advanced Materials* 23 (2011) 1154-1161.
- [20] B. Dan, G.C. Irvin, M. Pasquali, *ACS Nano* 3 (2009) 835-843.
- [21] D.-Y. Khang, J. Xiao, C. Kocabas, S. MacLaren, T. Banks, H. Jiang, Y.Y. Huang, J.A. Rogers, *Nano Letters* 8 (2007) 124-130.
- [22] D.J. Lipomi, M. Vosgueritchian, B.C. Tee, S.L. Hellstrom, J.A. Lee, C.H. Fox, Z. Bao, *Nat Nanotechnol* 6 (2011) 788-792.
- [23] D.J. Cohen, D. Mitra, K. Peterson, M.M. Maharbiz, *Nano Letters* 12 (2012) 1821-1825.
- [24] A.G. Nasibulin, A. Kaskela, K. Mustonen, A.S. Anisimov, V. Ruiz, S. Kivistö, S. Rackauskas, M.Y. Timmermans, M. Pudas, B. Aitchison, M. Kauppinen, D.P. Brown, O.G. Okhotnikov, E.I. Kauppinen, *ACS Nano* 5 (2011) 3214-3221.
- [25] K. Kim, K. Shin, J.H. Han, K.R. Lee, W.H. Kim, K.B. Park, B.K. Ju, J.J. Pak, *Electronics Letters* 47 (2011) 118-120.
- [26] S.M. Lyth, S.R.P. Silva, *Applied Physics Letters* 90 (2007) 173124.
- [27] A. Izadi-Najafabadi, T. Yamada, D.N. Futaba, M. Yudasaka, H. Takagi, H. Hatori, S. Iijima, K. Hata, *ACS Nano* 5 (2011) 811-819.
- [28] Z. Yang, T. Chen, R. He, G. Guan, H. Li, L. Qiu, H. Peng, *Advanced Materials* 23 (2011) 5436-5439.
- [29] G. Eda, G. Fanchini, M. Chhowalla, *Nat Nanotechnol* 3 (2008) 270-274.
- [30] X. Li, G. Zhang, X. Bai, X. Sun, X. Wang, E. Wang, H. Dai, *Nat Nanotechnol* 3 (2008) 538-542.
- [31] T. Ohta, A. Bostwick, T. Seyller, K. Horn, E. Rotenberg, *Science* 313 (2006) 951-954.

- [32] P.W. Sutter, J.I. Flege, E.A. Sutter, *Nat Mater* 7 (2008) 406-411.
- [33] K.S. Kim, Y. Zhao, H. Jang, S.Y. Lee, J.M. Kim, K.S. Kim, J.H. Ahn, P. Kim, J.Y. Choi, B.H. Hong, *Nature* 457 (2009) 706-710.
- [34] S. Bae, H. Kim, Y. Lee, X. Xu, J.S. Park, Y. Zheng, J. Balakrishnan, T. Lei, H.R. Kim, Y.I. Song, Y.J. Kim, K.S. Kim, B. Ozyilmaz, J.H. Ahn, B.H. Hong, S. Iijima, *Nat Nanotechnol* 5 (2010) 574-578.
- [35] P.A. Denis, F. Iribarne, *The Journal of Physical Chemistry C* 117 (2013) 19048-19055.
- [36] A.L. Dearden, P.J. Smith, D.-Y. Shin, N. Reis, B. Derby, P. O'Brien, *Macromolecular Rapid Communications* 26 (2005) 315-318.
- [37] Y. Li, Y. Wu, B.S. Ong, *J Am Chem Soc* 127 (2005) 3266-3267.
- [38] K. Ankireddy, S. Vunnam, J. Kellar, W. Cross, *Journal of Materials Chemistry C* 1 (2013) 572-579.
- [39] A. Kamyshny, M. Ben-Moshe, S. Aviezer, S. Magdassi, *Macromolecular Rapid Communications* 26 (2005) 281-288.
- [40] B.J. de Gans, P.C. Duineveld, U.S. Schubert, *Advanced Materials* 16 (2004) 203-213.
- [41] P.M. Harrey, B.J. Ramsey, P.S.A. Evans, D.J. Harrison, *Sensors and Actuators B: Chemical* 87 (2002) 226-232.
- [42] T. Mäkelä, S. Jussila, H. Kosonen, T.G. Bäcklund, H.G.O. Sandberg, H. Stubb, *Synthetic Metals* 153 (2005) 285-288.
- [43] D. Zielke, A.C. Hübler, U. Hahn, N. Brandt, M. Bartsch, U. Fügmann, T. Fischer, J. Veres, S. Ogier, *Applied Physics Letters* 87 (2005) -.
- [44] A.C. Huebler, F. Doetz, H. Kempa, H.E. Katz, M. Bartsch, N. Brandt, I. Hennig, U. Fügmann, S. Vaidyanathan, J. Granstrom, S. Liu, A. Sydorenko, T. Zillger, G. Schmidt, K. Preissler, E. Reichmanis, P. Eckerle, F. Richter, T. Fischer, U. Hahn, *Organic Electronics* 8 (2007) 480-486.
- [45] K. Suganuma, *Printing Technology, Introduction to Printed Electronics*, vol 74, Springer New York, 2014, pp. 23-48.

- [46] A. Blayo, B. Pineaux, Printing processes and their potential for RFID printing, Proceedings of the 2005 joint conference on Smart objects and ambient intelligence: innovative context-aware services: usages and technologies, ACM, Grenoble, France, 2005, pp. 27-30.
- [47] I. Park, S.H. Ko, H. Pan, C.P. Grigoropoulos, A.P. Pisano, J.M.J. Fréchet, E.S. Lee, J.H. Jeong, *Advanced Materials* 20 (2008) 489-496.
- [48] C.M. Sotomayor Torres, S. Zankovych, J. Seekamp, A.P. Kam, C. Clavijo Cedeño, T. Hoffmann, J. Ahopelto, F. Reuther, K. Pfeiffer, G. Bleidiessel, G. Gruetzner, M.V. Maximov, B. Heidari, *Materials Science and Engineering: C* 23 (2003) 23-31.
- [49] Z. Yin, Y. Huang, N. Bu, X. Wang, Y. Xiong, *Chinese Science Bulletin* 55 (2010) 3383-3407.
- [50] F.C. Krebs, *Solar Energy Materials and Solar Cells* 93 (2009) 394-412.
- [51] A.C. Siegel, S.T. Phillips, M.D. Dickey, N. Lu, Z. Suo, G.M. Whitesides, *Advanced Functional Materials* 20 (2010) 28-35.
- [52] J.E. Rogers, R. Ramadoss, P.M. Ozmun, R.N. Dean, *J. Micromech. Microeng.* 18 (2008) 015013.
- [53] I.E. Gonenli, Z. Celik-Butler, D.P. Butler, *Sensors Journal, IEEE* 11 (2011) 2318-2326.
- [54] D.J. Young, M.A. Zurcher, M. Semaan, C.A. Megerian, W.H. Ko, *IEEE Trans. Biomed. Eng.* 59 (2012) 3283-3292.
- [55] R. Bogue, *Sensor Review* 27 (2007) 7-13.
- [56] B.E. Boser, R.T. Howe, *Solid-State Circuits, IEEE Journal of* 31 (1996) 366-375.
- [57] D.V. Dao, K. Nakamura, T.T. Bui, S. Sugiyama, *Adv. Nat. Sci: Nanosci. Nanotechnol.* 1 (2010) 013001.
- [58] P.A. Wlodkowski, K. Deng, M. Kahn, *Sensors and Actuators A: Physical* 90 (2001) 125-131.
- [59] H.G. Yu, L. Zou, K. Deng, R. Wolf, S. Tadigadapa, S. Trolrier-McKinstry, *Sensors and Actuators A: Physical* 107 (2003) 26-35.
- [60] F.A. Levinzon, *Sensors Journal, IEEE* 6 (2006) 1164-1169.

- [61] T. Itoh, T. Kobayashi, H. Okada, T. Masuda, T. Suga, A digital output piezoelectric accelerometer for ultra-low power wireless sensor node, *Sensors*, 2008 IEEE, 2008, pp. 542-545.
- [62] C. Tse, Design of a Power Scalable Capacitive MEMS Accelerometer Front End, University of Toronto, 2013.
- [63] M. Bao, Analysis and Design Principles of MEMS Devices, Elsevier Science & Technology, Amsterdam, NL, 2005.
- [64] C. Liu, Foundations of MEMS, Prentice Hall, Upper Saddle River, N.J, 2011.
- [65] B.V. Amini, S. Pourkamali, F. Ayazi, A 2.5V 14-bit $\Sigma\Delta$ CMOS-SOI capacitive accelerometer, Solid-State Circuits Conference, 2004. Digest of Technical Papers. ISSCC. 2004 IEEE International, 2004, pp. 314-530 Vol.311.
- [66] J. Marek, MEMS for automotive and consumer electronics, Solid-State Circuits Conference Digest of Technical Papers (ISSCC), 2010 IEEE International, 2010, pp. 9-17.
- [67] T.J. Davis, G.J. Galvin, N.C. MacDonald, Micromechanical accelerometer for automotive applications, Google Patents, 2000.
- [68] W.J. Fleming, *Sensors Journal*, IEEE 1 (2001) 296-308.
- [69] C.R. Anson, System and method for automated display orientation detection and compensation, Google Patents, 2010.
- [70] Y. Abe, H. Inoue, M. Saitoh, M. Unuma, Free fall detection device, Google Patents, 2009.
- [71] P. McFadden, J. Smith, *Tribology international* 17 (1984) 3-10.
- [72] M. Angelo, *Sound & Vibration* 24 (1990) 20.
- [73] J.P. Lynch, K.J. Loh, *Shock and Vibration Digest* 38 (2006) 91-130.
- [74] S. Kim, S. Pakzad, D. Culler, J. Demmel, G. Fenves, S. Glaser, M. Turon, Health monitoring of civil infrastructures using wireless sensor networks, *Information Processing in Sensor Networks*, 2007. IPSN 2007. 6th International Symposium on, IEEE, 2007, pp. 254-263.
- [75] D.D. Mehta, Za, x00F, M. artu, S.W. Feng, H.A. Cheyne, R.E. Hillman, *Biomedical Engineering*, IEEE Transactions on 59 (2012) 3090-3096.

- [76] S. Patel, H. Park, P. Bonato, L. Chan, M. Rodgers, *Journal of neuroengineering and rehabilitation* 9 (2012) 21.
- [77] M. Trifunovic, A.M. Vadiraj, W.D. Van Driel, MEMS accelerometers and their bio-applications, *Thermal, Mechanical and Multi-Physics Simulation and Experiments in Microelectronics and Microsystems (EuroSimE), 2012 13th International Conference on, 2012*, pp. 1/7-7/7.
- [78] C.V.C. Bouten, K.T.M. Koekkoek, M. Verduin, R. Kodde, J.D. Janssen, *Biomedical Engineering, IEEE Transactions on* 44 (1997) 136-147.
- [79] Y.-J. Hong, I.-J. Kim, S.C. Ahn, H.-G. Kim, *Simulation Modelling Practice and Theory* 18 (2010) 446-455.
- [80] C.-C. Yang, Y.-L. Hsu, *Sensors* 10 (2010) 7772-7788.
- [81] M. Chang, *Review of clinical applications with human accelerometry*, ISSN, 2006.
- [82] I. López-Nava, A. Muñoz-Meléndez, Towards Ubiquitous Acquisition and Processing of Gait Parameters, in: G. Sidorov, A. Hernández Aguirre, C. Reyes García (Eds.), *Advances in Artificial Intelligence*, vol 6437, Springer Berlin Heidelberg, 2010, pp. 410-421.
- [83] R.J. Gibbons, *JOURNAL-AMERICAN COLLEGE OF CARDIOLOGY* 34 (1999) 912-945.
- [84] E.S. Winokur, D.D. He, C.G. Sodini, A wearable vital signs monitor at the ear for continuous heart rate and Pulse Transit Time measurements, *Engineering in Medicine and Biology Society (EMBC), 2012 Annual International Conference of the IEEE, 2012*, pp. 2724-2727.
- [85] D.G. Guo, F.E.H. Tay, L. Xu, L.M. Yu, M.N. Nyan, F.W. Chong, K.L. Yap, B. Xu, A Long-term Wearable Vital Signs Monitoring System using BSN, *Digital System Design Architectures, Methods and Tools, 2008. DSD '08. 11th EUROMICRO Conference on, 2008*, pp. 825-830.
- [86] F. Khoshnoud, C.W. de Silva, *IEEE Instrum. Meas. Mag.* 15 (2012) 14-24.
- [87] P.A. Shaltis, A. Reisner, H.H. Asada, Wearable, Cuff-less PPG-Based Blood Pressure Monitor with Novel Height Sensor, *Engineering in Medicine and Biology Society, 2006. EMBS '06. 28th Annual International Conference of the IEEE, 2006*, pp. 908-911.
- [88] N. Klejwa, R.G. Hennessy, J.W.P. Chen, R.T. Howe, A reel-to-reel compatible printed accelerometer, *TRANSDUCERS 2011, 16th International, Solid-State Sensors, Actuators and Microsystems Conference, 2011*, pp. 699-702.

- [89] A.C. Siegel, S.T. Phillips, M.D. Dickey, N. Lu, Z. Suo, G.M. Whitesides, *Adv. Funct. Mater.* 20 (2010) 28-35.
- [90] A.D. Mazzeo, W.B. Kalb, L. Chan, M.G. Killian, J.-F. Bloch, B.A. Mazzeo, G.M. Whitesides, *Adv. Mater.* 24 (2012) 2850-2856.
- [91] X. Liu, M. Mwangi, X. Li, M. O'Brien, G.M. Whitesides, *Lab on a Chip* 11 (2011) 2189-2196.
- [92] N. Yazdi, K. Najafi, *Microelectromechanical Systems, Journal of* 9 (2000) 544-550.
- [93] Y. Zhang, C. Lei, W.S. Kim, *Applied Physics Letters* 103 (2013) 073304.
- [94] D. Tobjörk, R. Österbacka, *Advanced Materials* 23 (2011) 1935-1961.
- [95] W. Wong, M. Chabiny, T.-N. Ng, A. Salleo, *Materials and Novel Patterning Methods for Flexible Electronics*, in: W. Wong, A. Salleo (Eds.), *Flexible Electronics*, vol 11, Springer US, 2009, pp. 143-181.
- [96] J. Kim, T.N. Ng, W.S. Kim, *App. Phy. Lett.* 101 (2012) 103308.
- [97] J. Kim, K. Wubs, B.S. Bae, W.S. Kim, *Sci. Tech. Adv. Mater.* 13 (2012) 035004.
- [98] Y. Hao, R. Foster, *Physiol Meas* 29 (2008) R27-56.
- [99] K.Z. Siejko, P.H. Thakur, K. Maile, A. Patangay, M.-T. Olivari, *Pacing and Clinical Electrophysiology* 36 (2013) 334-346.
- [100] F. Tjulkins, A.T. Nguyen, M. Andersen, K. Imenes, *MEMS Accelerometer-Based Heart Monitoring System with Myocardial Fixation*, in: Y. Dekhtyar, A. Katashev, L. Lancere (Eds.), *International Symposium on Biomedical Engineering and Medical Physics*, 10-12 October, 2012, Riga, Latvia, vol 38, Springer Berlin Heidelberg, 2013, pp. 19-22.
- [101] K. Pandia, S. Ravindran, R. Cole, G. Kovacs, L. Giovangrandi, *Motion artifact cancellation to obtain heart sounds from a single chest-worn accelerometer*, *Acoustics Speech and Signal Processing (ICASSP)*, 2010 IEEE International Conference on, 2010, pp. 590-593.
- [102] W.Q. Lindh, *Vital signs and measurements*, *Delmar's Comprehensive Medical Assisting: Administrative and Clinical Competencies*, Cengage Learning, 2009.

Appendix A.

Contributions to the Project during Master Thesis

1. Journal articles:

- a) Y. Zhang, T. Lei, and W.S. Kim*, "Design optimized membrane-based flexible paper accelerometer with silver nano ink" *Appl. Phys. Lett.* 103, 073304 (2013).
- b) Y Zhang, and W.S. Kim*, "Highly Sensitive Attachable Printed Sensor for Monitoring Vital Signs" *Soft Robotics* 1(2), pp. 132-135 (2014).

2. Conference presentation and proceedings:

- a) 2014 MRS Spring Meeting presentation (Z3.41/AA3.41)
Title: A Flexible Accelerometer System for Human Pulse Monitoring
Date & Location: Tuesday, April 22, 2014 in San Francisco, California, USA
- b) 2014 MRS Spring Meeting proceeding in press
Symposium Z - Bioelectronics—Materials, Processes and Applications
Title: A Flexible Accelerometer System for Human Pulse Monitoring